Original Article

TFAP2A-activated *ITGB4* promotes lung adenocarcinoma progression and inhibits CD4$^+$/CD8$^+$ T-cell infiltrations by targeting *NF-κB* signaling pathway

Cheng Pan[#], Zhibo Wang[#], Qi Wang[#], Hongshun Wang, Xiaheng Deng, Liang Chen, Zhihua Li

Department of Thoracic Surgery, The First Affiliated Hospital of Nanjing Medical University, Nanjing, China

Contributions: (I) Conception and design: C Pan, Z Li, L Chen; (II) Administrative support: Z Li, X Deng; (III) Provision of study materials or patients: Z Li, L Chen; (IV) Collection and assembly of data: C Pan, Z Wang, Q Wang, X Deng, H Wang; (V) Data analysis and interpretation: C Pan, Z Wang, Q Wang, H Wang; (VI) Manuscript writing: All authors; (VII) Final approval of manuscript: All authors.

[#]These authors contributed equally to this work.

Correspondence to: Zhihua Li, MD; Liang Chen, MD. Department of Thoracic Surgery, The First Affiliated Hospital of Nanjing Medical University, No. 300, Guangzhou Road, Nanjing 210029, China. Email: lizhihua@njmu.edu.cn; clbright0909@njmu.edu.cn.

Background: Immune-associated genes play vital roles in the tumorigenesis, progression and immunotherapy responses of malignant tumors. This study aimed to comprehensively evaluate the role and mechanism of novel immune-associated gene integrin β4 (*ITGB4*) in the progression and immune microenvironment of lung adenocarcinoma (LUAD).

Methods: There were 770 immune-associated genes curated from NanoString PanCancer Immune Profiling Panel. Differentially expressed immune-related genes were initially screened using transcriptome data from 57 paired LUAD samples in The Cancer Genome Atlas (TCGA) and 15 paired LUAD samples in GSE31210, and were further validated in 19 paired LUAD samples from our institution. Log-rank test was adopted to identify LUAD prognosis associated genes. Among the identified differentially expressed genes, *ITGB4* was ultimately chosen for further analysis. Subsequently, the functionality and mechanisms of *ITGB4* were investigated in two LUAD cell lines, A549 and PC9, which exhibited relatively high expression levels of *ITGB4*. Following this, the impact of *ITGB4* on the proliferation and metastasis of LUAD *in vivo* was evaluated using nude mice. Additionally, its effect on T cell infiltration was studied using immunocompetent C57BL/6J mice.

Results: *ITGB4* was found to be significantly up-regulated in LUAD and associated with an unfavorable prognosis. Functionally, *ITGB4* could promote LUAD cell proliferation, migration and invasion. Consistently, *in vivo* experiments demonstrated that *ITGB4* knockdown suppressed LUAD tumor growth and metastasis. Additionally, *ITGB4* could suppress CD4$^+$ and CD8$^+$ T-cell infiltrations in LUAD cells. Mechanistically, *ITGB4* could activate the *NF-κB* signaling pathway by interacting with *IκBα*. Furthermore, *TFAP2A* could directly bind to the *ITGB4* promoter and transcriptionally activate *ITGB4* in LUAD cells. In addition, *laminin-5*, a ligand of *ITGB4*, was found to promote LUAD progression by activating the *ITGB4* signaling.

Conclusions: *ITGB4* was transcriptionally activated by *TFAP2A*, and could promote LUAD progression and inhibit CD4$^+$/CD8$^+$ T-cell infiltrations by activating the *NF-κB* signaling pathway. *ITGB4* may serve as a potential immunotherapeutic target of LUAD.

Keywords: Immune-associated genes; lung adenocarcinoma (LUAD); T-cell infiltrations; *NF-κB* signaling; transcription factor

Submitted Jan 15, 2024. Accepted for publication Jul 26, 2024. Published online Sep 10, 2024.
doi: 10.21037/tlcr-24-50
View this article at: https://dx.doi.org/10.21037/tlcr-24-50

Introduction

Lung cancer remains the leading cause of cancer death globally, comprising 18% of total cancer deaths (1). Among the various subtypes of lung cancer, lung adenocarcinoma (LUAD) is the most prevalent one, accounting for around 40% of all lung cancer cases (2). Although advancements in cancer immunotherapy have improved the prognosis of LUAD patients, the 5-year survival rate of patients remains low (3,4).

The tumor immune microenvironment (TIME) plays crucial roles in the progression of malignant tumors (5). Among the immune cells in the TIME, T cells represent the prevalent cell type and are closely associated with cancer immunotherapy (6,7). In lung cancer, higher $CD3^+$, $CD4^+$ or $CD8^+$ T-cell infiltrations are associated with a favorable prognosis (8-12). In recent years, immunotherapies have shown unexpected superiority to conventional chemotherapies in LUAD (13). However, due to the resistance to immunotherapy, the overall response rate of anti-programmed cell death protein 1 (PD-1)/programmed death-ligand 1 (PD-L1) treatment remains only ~15% (14). Additionally, the occurrence of severe immune-related adverse events has significantly impacted treatment effectiveness (15). Therefore, identification of novel immune-associated genes that affect the progression and TIME of LUAD may be of great importance.

Immune-associated genes play fundamental roles in regulating tumor progression and immune responses. In a previous study, a total of 770 immune-associated genes were provided by nCounter® PanCancer Immune Profiling Panel (NanoString), a unique 770-plex gene expression panel measuring tumor immune responses based on NanoString technology (Seattle, USA) (16). The platform provides a detailed list of these immune-related genes along with probe information and sufficient functional annotations. Their important role in tumor progression has been widely established. For instance, Lu *et al.* demonstrated that *NLRP3* promoted lymphoma growth and suppressed anti-tumor immunity by upregulating PD-L1 in the tumor microenvironment (17). Ma *et al.* revealed that *IL-17A* exerted a tumor-promoting effect by suppressing $CD8^+$ T-cell responses (18). Tosti and colleagues demonstrated that the immune-associated gene *IL22* was produced by $CD4^+$ and $CD8^+$ polyfunctional T cells and was associated with a favorable clinical outcome by enhancing T-cell responses in colorectal cancer (19). These studies collectively emphasize the critical roles of immune-associated genes in tumor progression and the immune microenvironment. In this research, we conducted a thorough analysis aimed at identifying novel immune-associated genes that influence the progression and TIME of LUAD. Among these genes, integrin β4 (*ITGB4*) was notably up-regulated in LUAD and linked to an unfavorable prognosis. Therefore, we speculate that *ITGB4* may act as an oncogenic gene to promote the progression of lung adenocarcinoma and inhibit tumor immunity. However, its specific function and mechanism need further investigation.

Functional experiments and animal models were conducted to elucidate the role of *ITGB4* in promoting the progression of lung adenocarcinoma both *in vivo* and *in vitro*. RNA sequencing (RNA-seq) analysis, Kyoto Encyclopedia of Genes and Genomes (KEGG) pathway enrichment analysis, and western blot assays were employed to unveil *ITGB4*'s capacity to activate the *NF-κB* signaling pathway. Immunoprecipitation (IP) assays, mass spectrometry analysis, and co-immunoprecipitation (co-IP) assays demonstrated direct binding between *ITGB4* and IκBα, a pivotal protein in the *NF-κB* pathway. Immunohistochemistry (IHC) of lung adenocarcinoma samples and an immunocompetent mouse model showcased ITGB4's ability to suppress $CD4^+$ and $CD8^+$ T-cell infiltrations in LUAD cells. Luciferase reporter assays and chromatin IP (ChIP) assays unveiled TFAP2A's direct

Highlight box

Key findings

- Integrin β4 (*ITGB4*) is an oncogene for lung adenocarcinoma (LUAD).

What is known and what is new?

- Upregulation of *ITGB4* has been observed in various malignant tumors, including glioma, gastric and cervical cancer. In lung cancer, aberrant *ITGB4* expression was associated with decreased overall survival. However, the specific functions and underlying mechanisms of *ITGB4* in LUAD progression are yet to be fully elucidated.
- Functional assays indicated that *ITGB4* could promote LUAD progression *in vitro* and *in vivo*. Mechanistically, *ITGB4* could activate the *NF-κB* signaling pathway by interacting with *IκBα*. Additionally, *ITGB4* could suppress $CD4^+$ and $CD8^+$ T-cell infiltrations in LUAD cells. Lastly, *TFAP2A* could directly bind to the *ITGB4* promoter and transcriptionally activate *ITGB4* in LUAD cells.

What is the implication, and what should change now?

- *ITGB4* exerts an oncogenic role in LUAD. It may serve as a potential immunotherapeutic target of LUAD.

binding to the *ITGB4* promoter, thereby transcriptionally activating *ITGB4* in LUAD cells.

In this study, we hypothesized that transcription factor *TFAP2A*-activated *ITGB4* may promote lung adenocarcinoma progression and inhibit $CD4^+$/$CD8^+$ T-cell infiltrations through targeting *NF-κB* signaling pathway by interacting with *IκBα*. *ITGB4* may serve as a potential immunotherapeutic target of LUAD. We present this article in accordance with the MDAR reporting checklist (available at https://tlcr.amegroups.com/article/view/10.21037/tlcr-24-50/rc).

Methods

Patients and tissue specimens

In the present study, the transcriptome data of 57 paired LUAD samples from The Cancer Genome Atlas (TCGA) (https://portal.gdc.cancer.gov/) and 15 paired LUAD samples from GSE31210 (https://www.ncbi.nlm.nih.gov/gds) were used to screen differentially expressed genes. Survival analysis was performed based on 500 patients with LUAD from TCGA and 226 patients with LUAD from GSE31210. A total of 20 paired LUAD samples were collected from The First Affiliated Hospital of Nanjing Medical University between January 2019 and January 2020. All patients were diagnosed with primary LUAD and had not received any type of preoperative anti-tumor therapies. Written informed consent was obtained from all individual participants. All the procedures involving patient samples were compliant with all relevant ethical regulations and approved by the Research Ethics Committee of The First Affiliated Hospital of Nanjing Medical University (Approval No. 2019-SR-123). The study was conducted in accordance with the Declaration of Helsinki (as revised in 2013). The characteristics of the study subjects are shown in Table S1.

RNA-seq

Total RNA was isolated from cells using TRIzol® reagent (Invitrogen, CA, USA). Then, RNA was treated using a Ribo-off rRNA Depletion Kit (Vazyme, Nanjing, China) to remove ribosomal RNA before generating the RNA-seq library. The RNA-seq library was deep sequenced with an illumina NovaseqTM6000 instrument (illumina, San Diego, USA). The reads were mapped to the human reference genome (Homo sapiens. GRCh38). Bcl2FastQ, FastQC, and DESeq were used for data processing and analyses.

Cell culture

A human normal bronchial cell line 16HBE (CVCL_0112), five human lung adenocarcinoma cell lines H1299 (CVCL_0060), H1975 (CVCL_1511), A549 (CVCL_0023), H358 (CVCL_1559), PC9 (CVCL_B260), and a Lewis lung carcinoma (LLC; LL/2) (CVCL_4358) cell line were obtained from the Institute of Biochemistry and Cell Biology of the Chinese Academy of Sciences, Shanghai, China. All cell lines were tested by short tandem repeat (STR) (Shanghai Zhong Qiao Xin Zhou Biotechnology, Shanghai, China). Cells were cultured in the RPMI-1640 medium supplemented with 1% penicillin-streptomycin and 10% fetal bovine serum (FBS). All cell lines were incubated at 37 ℃ with 5% CO_2.

Plasmid construction, small interfering RNA (siRNA) interference and lentiviral infection

To construct *ITGB4*-overexpressing plasmids (named *ITGB4* OE), human *ITGB4* complementary DNA (cDNA) was synthesized and cloned into the pcDNA3.1(+) vector (Invitrogen), while empty plasmids were used as a control (named vector). Transfection was performed with Lipofectamine® 2000 (Invitrogen).

ITGB4-knockdown lentivirus was designed and constructed by Shanghai GeneChem (Shanghai, China). Short hairpin RNAs (shRNAs) against *ITGB4* were cloned into the GV248 lentiviral vector (GeneChem). The scrambled shRNA sequence was also cloned into the GV248 vector and was used as a negative control [named sh-negative control (sh-NC)]. The lentivirus vectors were transfected into A549, PC9, and LLC cells using 7 μg/mL polybrene (Sigma, St. Louis, USA). Following transfection for 2 days, the cells were subjected to selection with 3 μg/mL puromycin (Sigma) for 2 weeks to establish stable cell lines exhibiting *ITGB4* knockdown.

The siRNAs (named si-TFAP2A) and overexpression plasmid for *TFAP2A* (named *TFAP2A* OE) were synthesized by GenePharma (Shanghai, China) and transfected as aforementioned. All the sequences used in the present study are listed in Table S2. Sh-ITGB4#1 (human) (named sh-ITGB4) and sh-ITGB4 (mouse) (named LLC-sh-ITGB4) were utilized in *in vivo* assays.

RNA extraction and quantitative reverse transcription polymerase chain reaction (qRT-PCR) assays

Total RNA was extracted from the cell lines using TRIzol® reagent (Invitrogen) and reverse transcribed using a PrimeScript Reverse Transcription Kit (Takara, Tokyo, Japan) according to the instructions. qRT-PCR was conducted on a StepOnePlus™ Real-Time PCR System (Thermo, Waltham, USA). Relative mRNA expression, normalized to β-actin, was calculated using the $2^{-\Delta\Delta Ct}$ method. The primers utilized in this study are listed in Table S3.

Protein isolation and western blot assays

Total protein was isolated from A549 and PC9 cells using RIPA buffer (Beyotime, Shanghai, China). Bicinchoninic acid assay (KeyGEN, Nanjing, China) was used to determine the protein concentration. After being separated by the sodium dodecyl sulfate-polyacrylamide gel electrophoresis (SDS-PAGE), the lysates of protein were transferred to the polyvinylidene fluoride (PVDF) membranes. Then, the membranes were incubated at 4 ℃ overnight with specific primary antibodies. Afterwards, the blots were incubated with a horseradish peroxidase (HRP)-conjugated anti-rabbit secondary antibody for 2 hours. Protein bands were visualized using an enhanced chemiluminescence (ECL) substrate kit (NCM Biotech, Suzhou, China). The antibodies utilized in this study are listed in Table S4.

Subcellular fractionation

Nuclear and cytoplasmic fractions from A549 and PC9 cells were isolated using Nuclear and Cytoplasmic Extraction Reagents (Thermo Fisher Scientific) following the manufacturer's descriptions. The subcellular localization of proteins was determined by western blotting. Anti-Lamin B1 antibody and anti-GAPDH (glyceraldehyde-3-phosphate dehydrogenase) antibody were used as loading controls for the nuclear and cytoplasmic fractions, respectively.

Co-IP assay, IP assay and mass spectrometry

Co-IP assays were conducted using the Pierce Co-IP kit (Thermo) according to the manufacturer's descriptions. Cell extracts were prepared in IP lysis buffer and incubated overnight at 4 ℃ with either immunoglobulin G (IgG) (5 μg) or primary antibodies (5 μg), including anti-ITGB4 antibody and anti-IκBα antibody. Total extracts were then incubated with protein A/G agarose beads (Thermo) for 2 hours. The protein A/G agarose beads were collected and washed with lysis buffer. Immunoprecipitated proteins were resolved by SDS-PAGE and analyzed by western blot assays as described above.

In addition, IP assay was also performed using the Pierce Co-IP kit (Thermo). A549 cell extracts were prepared in IP lysis buffer and incubated overnight at 4 ℃ with either anti-IgG or anti-ITGB4 antibodies (5 μg). Total extracts were then incubated with protein A/G agarose beads (Thermo) for 2 hours. The beads were subsequently washed thoroughly, and the IP proteins were analyzed by mass spectrometry (Applied Protein Technology, Shanghai, China). Mass spectrometry was analyzed using Proteome Discoverer software with the UniProtKB human database (UniProt Homo sapiens 207393_20230103).

Cell Counting Kit-8 (CCK-8) and colony formation assays

The CCK-8 assay was performed using the CCK-8 solution (Dojindo, Tokyo, Japan) according to a protocol of the manufacturer. Cells were seeded into 96-well plates for 2×10^3 cells/100 μL/well. After being incubated for 0, 24, 48, 72 and 96 hours, the cells were treated with 10 μL/well of the CCK-8 solution to measure the cell viability at an absorbance of 450 nm using the microplate reader.

For the colony formation assay, LUAD cells were seeded into 6-well plates at a density of 1×10^3 cells per well and cultured in an incubator at 37 ℃ with 5% CO_2 for 14 days. The colonies were set with 4% paraformaldehyde and then stained with 0.1% crystal violet (Beyotime). The number of colonies containing more than 50 cells was counted in each well. All experiments were repeated three times.

5-ethynyl-2-deoxyuridine (EdU) assay

The EdU assay kit (RiboBio, Guangzhou, China) was used to assess the proliferation ability of cells following the recommendation of the manufacturer. Cells were seeded into 48-well plates and cultured for 24 hours. Then, 50 μM of EdU solution was added into the plate, and cells were incubated for 2 hours at 37 ℃ with 5% CO_2. Subsequently, cells were fixed with 4% paraformaldehyde for 30 min and permeabilized with 0.5% Triton X-100 for 10 min. Next, cells were stained with Apollo, and 4',6-diamidino-2-phenylindole (DAPI) was used to label cell nuclei.

The EdU-positive cells were observed under fluorescent microscopy and the proliferation rate was calculated in five randomly selected fields.

Cell migration and invasion assays

The migration and invasion abilities of LUAD cells were determined using transwell chambers (8 μm; Corning, Elmira, USA). Cells were seeded into 200 μL serum-free medium in the upper transwell chamber for 5×10^4 cells per chamber, while the lower chamber was filled with 600 μL RPMI-1640 or Dulbecco's Modification of Eagle's Medium (DMEM) supplemented with 10% FBS. For cell invasion assay, the upper chamber was coated with the Matrigel (Corning), which was the only difference with cell migration assay. After 2 days of incubation, cells were set with 4% paraformaldehyde and stained with 0.1% crystal violet (Beyotime). The non-migrated or non-invaded cells on the upper membrane of the insert chamber were eliminated using a cotton tip. The migrative or invasive ability of LUAD cells was determined by photographing the stained cells with an inverted microscope and counting in five randomly selected fields. All the experiments were performed in triplicate.

Wound healing assay

LUAD cells were seeded in 6-well plates at 80% confluency, and a linear scratch wound was created in the cell monolayers through a 200-μL pipette tip. Subsequently, the cells were cultured in medium without FBS. After washing the A549 and PC9 cells with phosphate buffer saline (PBS) to remove debris and floating cells, each wound was imaged at 0 and 48 hours using an inverted microscope.

ChIP assay

ChIP assay was performed using the Pierce Agarose ChIP Kit (Thermo Fisher Scientific) following the instructions of the manufacturer. A549 and PC9 cells were grown to about 90% confluence in a 10-cm culture dish and treated with 1% formaldehyde to produce DNA-protein cross-links. Cell lysates were sonicated to fragment chromatin DNA into 200–1,000 bp fragments. Equal amounts of chromatin supernatants were then subjected to IP using 2 μg of anti-TFAP2A antibody or anti-IgG antibody along with protein A/G magnetic beads. The protein/DNA complexes were subsequently de-crosslinked to release the DNA, and the enriched DNA fragments were analyzed by PCR. The sequences of the primers for ITGB4 were as follow: forward, 5'-AGGCCCCTCAGGCAAGCT-3' and reverse, 5'-GGAAGGAGTCCCAGTTTG-3'.

Luciferase reporter assay

The *TFAP2A*-binding motif within the promoter region of *ITGB4* was identified using JASPAR (http://jaspar.genereg.net/). The *ITGB4* promoter was amplified using PCR and cloned into the pGL3-basic luciferase vector (Promega Corporation, Madison, USA), and this construct was designated as ITGB4-WT. Subsequently, the *TFAP2A*-binding motif was removed from the *ITGB4* promoter vector using PCR-mediated mutagenesis, and this construct was named ITGB4-MUT. Additionally, *NF-κB* luciferase reporter constructs were obtained from Promega Corporation. All vectors were verified by sequencing, and their luciferase activities were measured using a Dual-Luciferase Reporter Assay Kit (Promega Corporation).

Animal studies

All animal experiments were performed under a project license (Approval No. IACUC-2208008) granted by the Ethics Committee of Nanjing Medical University, in compliance with the guidelines of the Ethics Committee of Nanjing Medical University for the care and use of animals. Human endpoints were applied when mice lost 20% of their initial body weight. The well-being and behavior of the animals were monitored every 2 days throughout the study period. To ensure humane treatment, all mice were administered 2% pentobarbital sodium (40 mg/kg) via intraperitoneal injection to induce deep anesthesia. Subsequently, euthanasia was performed through cervical dislocation. Specific criteria were utilized to confirm animal death, including the absence of breathing, heartbeat, corneal reflexes, muscle tone, and mucosal color. The maximum allowable tumor size throughout the study was limited to 1.5 cm^3.

For the xenograft assay, 20 male BALB/c nude mice (4 weeks old) were procured from the Shanghai Laboratory Animal Center (Chinese Academy of Sciences, Shanghai, China) and maintained under specific pathogen-free conditions (temperature: 25 ℃; humidity: 50%; light/dark cycle: 12/12 hours) with access to sterilized fodder and purified water. A total of 3×10^6 stable cells (either A549-sh-NC or A549-sh-ITGB4) were suspended in 200 μL PBS

and subcutaneously injected into the right flanks of the nude mice. The sh-ITGB4#1 was used in the following assays *in vivo* due to its higher knockdown efficiency. Tumor growth was monitored every 3 days, and tumor volumes were calculated using the formula: volume (cm^3) =0.5 × length × $width^2$. After a 27-day period following injection, the mice were euthanized, and the growth of subcutaneous tumors was assessed. Tumor tissues were collected and preserved for subsequent experiments.

For the pulmonary metastasis analysis, A549-sh-NC or A549-sh-ITGB4 cells were labeled with firefly luciferase. Next, 100 µL of cell suspension (2×10^6 cells) was injected into the tail veins of mice, with three mice in each group. Pulmonary metastasis was monitored Using a Xenogen IVIS Spectrum Imaging System (PerkinElmer, Waltham, USA). After 5 weeks, mice were sacrificed, and lungs were surgically dissected. The numbers of lung metastatic nodules were counted and validated using hematoxylin and eosin (HE)-stained sections by microscopy.

For the immunocompetent mouse model, 20 female C57BL/6J mice (6 weeks old) were purchased from the Shanghai Laboratory Animal Center (Chinese Academy of Sciences) and maintained under specific pathogen-free conditions. A total of 3×10^6 stable LLC-sh-NC or LLC-sh-ITGB4 cells suspended in 200 µL PBS were subcutaneously injected into the right flanks of the mice. The tumor volume was assessed every 3 days using the formula: tumor volume (cm^3) =0.5 × length × $width^2$. All the tumors were harvested and weighed 24 days after injection, and the tumor tissues were immediately preserved for further experiments.

Flow cytometric analysis of C57BL/6J mouse tumors

Tumor samples were dissociated into small fragments using scalpels, and digested in DMEM containing 2% FBS, collagenase IV (Millipore, Billerica, USA) and DNase I (Millipore). Next, the cells were filtered through a strainer (Thermo) and washed with PBS. Cell surface staining was performed in fluorescence-activated cell sorting (FACS) buffer (PBS supplemented with 2% FBS). All cells were resuspended in a diluted 100 µL antibodies solution. Next, the cells were analyzed using a CytoFLEX Flow Cytometer (Beckman Coulter, Inc., Pasadena, USA), and data were evaluated using FlowJo v10.8.1 software (BD Biosciences, San Jose, USA). The antibodies for mouse tumor-infiltrating lymphocyte (TIL) staining were as follows: allophycocyanin (APC) anti-mouse CD4 antibody (dilution 1:100; cat. no. 100411; BioLegend, Inc., San Diego, USA), AlexaFluor-647 anti-mouse CD8a antibody (dilution 1:100; cat. no. 100727; BioLegend, Inc.) and fluorescein isothiocyanate (FITC) anti-mouse CD45 antibody (dilution 1:100; cat. no. 157213; BioLegend, Inc.).

IHC analysis

Formalin-fixed and paraffin-embedded specimens were sectioned into 4-µm-thick slices. After deparaffinization in xylene and gradual rehydration with ethanol, the sections were treated with citrate buffer for antigen retrieval. Subsequently, the sections were incubated overnight at 4 ℃ with the primary antibodies. Two experienced pathologists, blinded to the clinical data of the patients, independently assessed and scored the immunostained sections. Staining intensity was scored as follows: 0 (–, no staining), 1 (+, weak staining), 2 (++, moderate staining), and 3 (+++, strong staining). The IHC score, ranging from 0 to 300, was calculated by multiplying the staining intensity and the percentage of positive cells. Based on the cutoff value of 150 for ITGB4 expression in tumor tissues, the 20 patients with LUAD were divided into a high ITGB4 expression group (IHC score >150) and a low ITGB4 expression group (IHC score ≤150).

Statistical analysis

In the current study, differential gene expression analysis was performed using paired Student's *t*-test. Log-rank test was adopted to evaluate the associations between immune-associated genes and LUAD prognosis. KEGG pathway enrichment and Gene Ontology (GO) analyses were performed using DAVID Bioinformatics Resources 6.8 (20). Student's *t*-test or one-way ANOVA was used to compare the differences between experimental groups. Pearson correlation coefficient was employed to assess the correlations between transcription factor levels and ITGB4 expression. All these statistical evaluations were completed with R 3.6.0 and GraphPad Prism (6.01). A P value of <0.05 was considered statistically significant.

Results

ITGB4 is up-regulated in LUAD tumor tissues, and patients with higher ITGB4 expression have an inferior prognosis

Out of the 770 immune-related genes from NanoString (table available at https://cdn.amegroups.cn/static/public/

tlcr-24-50-1.pdf), 78 genes exhibited abnormal upregulation in both TCGA database (57 paired LUAD samples) and GSE31210 dataset (15 paired LUAD samples). Remarkably, 12 of these genes were found to be significantly associated with poor LUAD prognosis in both datasets (*Figure 1A*). Among them, *ITGB4* was known to take part in a variety of biological processes, including immune responses, epithelial cell senescence, and airway inflammation (21-23). Based on the CancerSEA database (http://biocc.hrbmu.edu.cn/CancerSEA/), we found that *ITGB4* was related to several functional aspects of LUAD cells, especially inflammation and metastasis (Figure S1). As a result, the current study focused on investigating the functions of *ITGB4*. Expression analysis revealed significantly higher levels of *ITGB4* in LUAD tumor tissues compared with those in adjacent normal tissues in both TCGA database (*Figure 1B*) and the GSE31210 dataset (*Figure 1C*). These results were further validated in the current dataset, namely JSPH (Jiangsu Province Hospital) data, consisting of 19 paired LUAD samples (*Figure 1D*). Importantly, LUAD patients with higher *ITGB4* expression had worse outcomes {TCGA: hazard ratio (HR) =1.61 [95% confidence interval (CI): 1.21–2.18], P=0.001, *Figure 1E*; GSE31210: HR =2.04 (95% CI: 1.03–3.88), P=0.04, *Figure 1F*}. This finding was further confirmed in 69 advanced LUAD patients (stage III–IV) from the GSE68465 [HR =2.16 (95% CI: 1.40–4.00), P=0.002, Figure S2A] and 719 LUAD patients from the Kaplan-Meier plotter database (http://kmplot.com/analysis/) [HR =1.92 (95% CI: 1.53–2.44), P<0.001, Figure S2B]. Additionally, IHC performed on 20 paired LUAD samples indicated that tumor tissues had higher *ITGB4* IHC scores than the adjacent normal tissues (*Figure 1G,1H*).

ITGB4 promotes LUAD cell proliferation, migration and invasion in vitro

The expression of *ITGB4* in LUAD cell lines was significantly higher compared to the normal bronchial cell line (*Figure 2A*). The use of shRNAs effectively reduced *ITGB4* expression, while the *ITGB4* overexpression plasmid sufficiently increased *ITGB4* expression (*Figure 2B*). The sh-ITGB4#1 (named sh-ITGB4) was used in the following assays *in vivo* due to its higher knockdown efficiency. The CCK-8 assay results revealed a notable decrease in the relative number of viable LUAD cells upon *ITGB4* downregulation. Conversely, overexpression of *ITGB4* led to a relative increase in the number of viable cells (*Figure 2C,2D*). Silencing of *ITGB4* significantly reduced the number and size of cell colonies, while *ITGB4* overexpression showed opposite effects (*Figure 2E,2F*). Furthermore, *ITGB4* knockdown significantly inhibited the proliferation of LUAD cell in EdU assay (*Figure 2G*). On the contrary, *ITGB4* overexpression promoted the proliferation of A549 and PC9 cells (*Figure 2H*). Overall, these results indicated that *ITGB4* could facilitate the proliferation of LUAD cells *in vitro*.

In addition, transwell assay suggested that inhibition of *ITGB4* significantly reduced the migration and invasion of LUAD cells (*Figure 3A*). Overexpression of *ITGB4* led to a notable increase of their migratory and invasive abilities (*Figure 3B*). Consistently, in the wound healing assay, *ITGB4* silencing remarkably suppressed LUAD cell migration, while *ITGB4* overexpression had the opposite effects (*Figure 3C,3D*). These results indicated that *ITGB4* could exert an oncogenic effect on the proliferation, migration and invasion of LUAD cells.

ITGB4 promotes LUAD cell tumorigenesis and metastasis in vivo

To investigate the oncogenic role of *ITGB4* in LUAD tumors *in vivo*, a nude mouse xenograft model was established using stable A549-sh-ITGB4 cells. Knockdown of *ITGB4* significantly inhibited the growth of lung adenocarcinoma xenografts (*Figure 4A*). Compared to the control group, the A549-sh-ITGB4 group exhibited significantly lower tumor volumes and weights (*Figure 4B,4C*). IHC staining showed a reduced level of Ki-67 in the ITGB4-silencing group (*Figure 4D*). In the tail vein tumor metastasis models, *in vivo* bioluminescence imaging demonstrated significantly lower fluorescence intensity and proportion in the lungs with *ITGB4* inhibition (*Figure 4E*). Furthermore, *ITGB4* knockdown resulted in a significant reduction in the number of metastatic lung nodules (*Figure 4F,4G*). Collectively, these findings suggest that *ITGB4* could promote the growth and metastasis of LUAD tumors *in vivo*.

ITGB4 activates the NF-κB signaling pathway by interacting with IκBα

To investigate the molecular mechanism underlying the oncogenic role of *ITGB4* in LUAD, RNA-seq analysis was performed to compare the gene transcription profiles of A549-sh-NC and A549-sh-ITGB4 cells. The analysis identified 862 up-regulated genes and 674 down-regulated

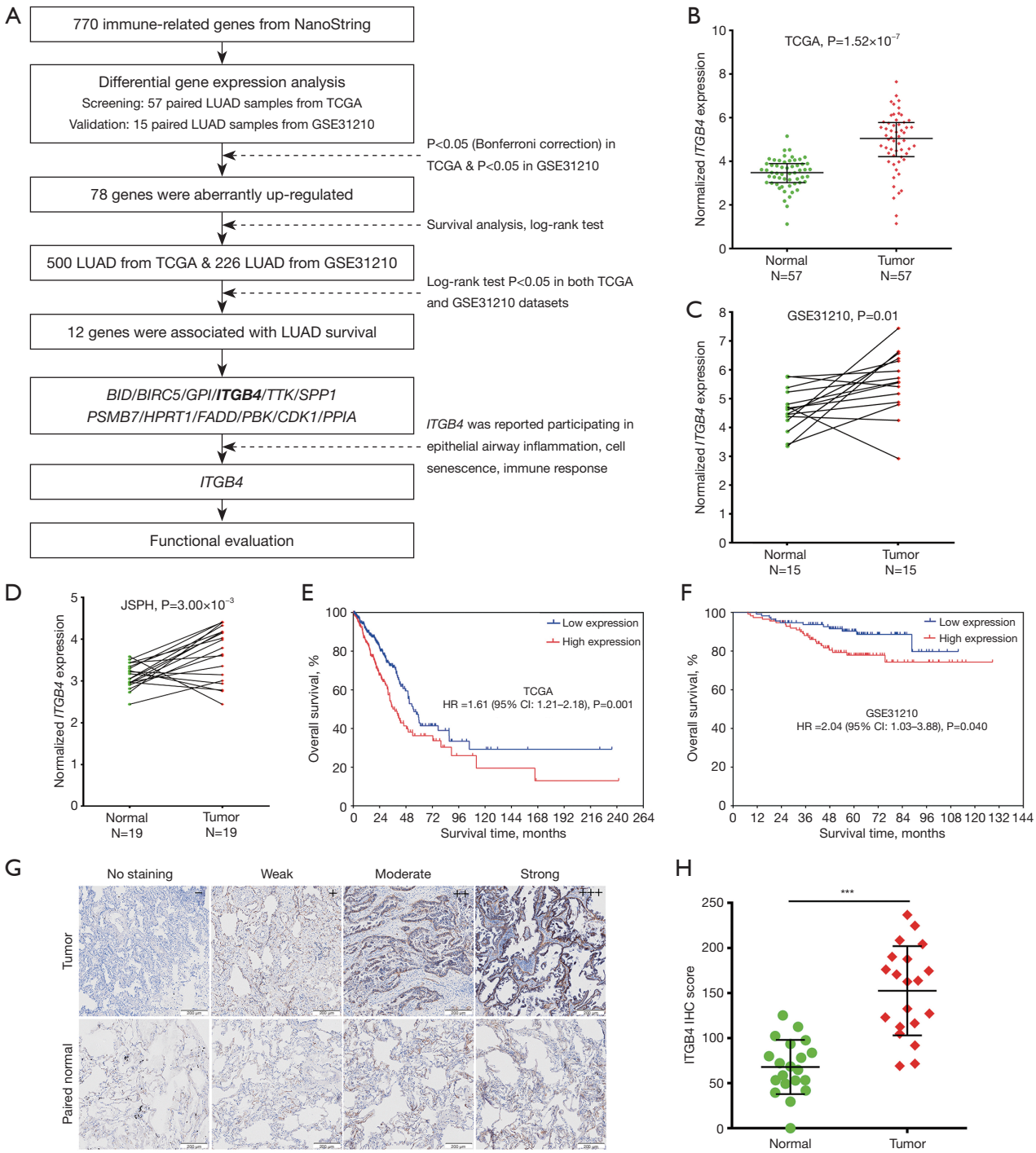

Figure 1 *ITGB4* is up-regulated in LUAD tumor tissues, and patients with higher *ITGB4* expression have an inferior prognosis. (A) Flowchart of the present study. (B-D) *ITGB4* was significantly up-regulated in LUAD compared with adjacent normal tissues in TCGA (B), GSE31210 (C) and JSPH (D) databases. (E,F) Patients with LUAD exhibiting a higher *ITGB4* expression had a worse prognosis in TCGA (E) and GSE31210 (F) datasets. (G,H) IHC analysis of *ITGB4* expression in 20 paired LUAD samples; (G) representative staining images of *ITGB4* expression were scored as follows: –, no staining; +, weak staining; ++, moderate staining; and +++, strong staining. Scale bar, 200 μm; (H) evaluation of the IHC score of *ITGB4* expression. Values are expressed as the means ± SDs. ***, P<0.001. LUAD, lung adenocarcinoma; TCGA, The Cancer Genome Atlas; HR, hazard ratio; CI, confidence interval; IHC, immunohistochemistry; JSPH, Jiangsu Province Hospital; SDs, standard deviations.

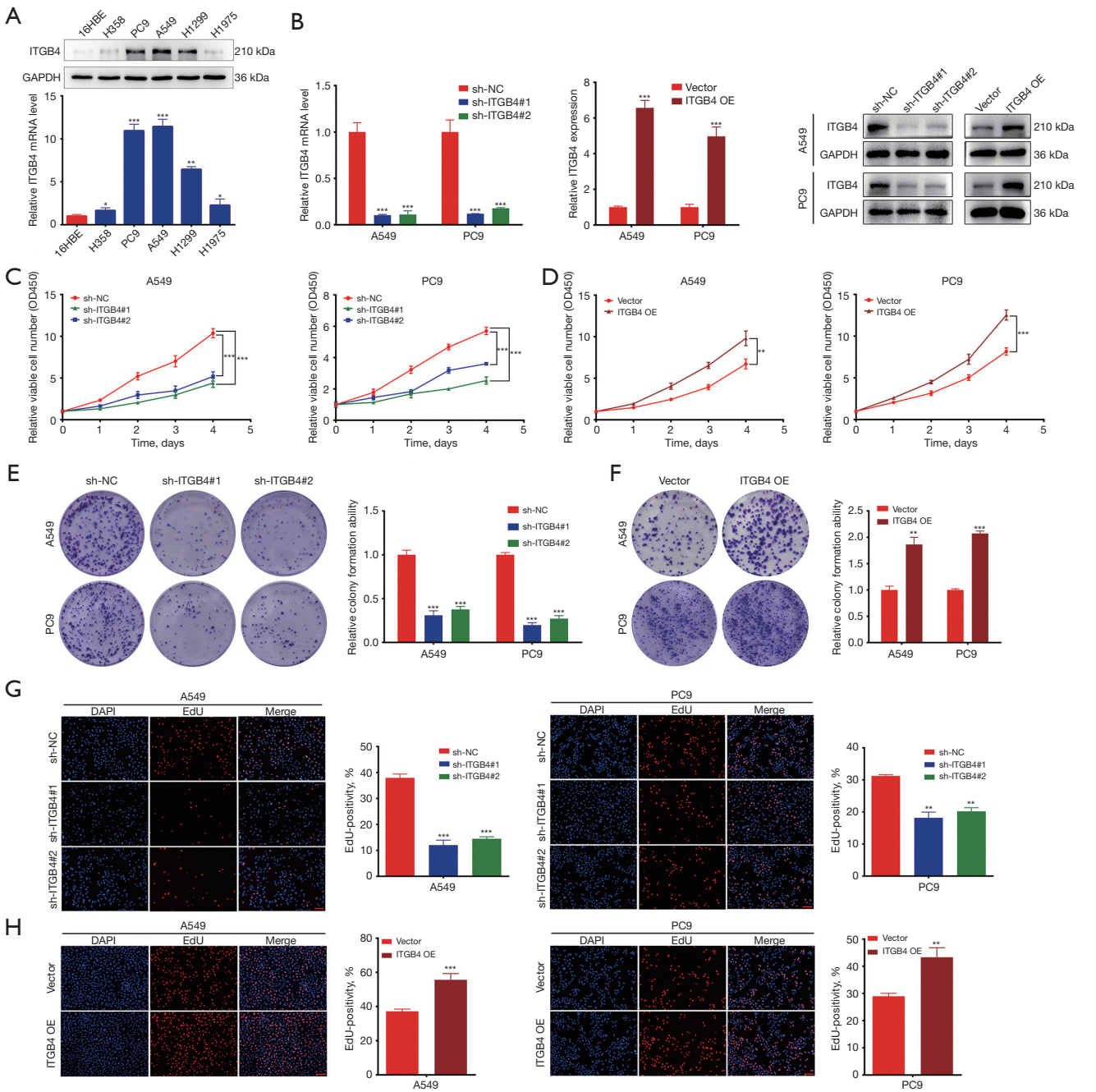

Figure 2 *ITGB4* promotes LUAD cell proliferation *in vitro*. (A) Relative *ITGB4* expression in cell lines was determined by qRT-PCR and western blot assays. (B) The efficiency of *ITGB4* knockdown and overexpression in A549 and PC9 cells was verified by qRT-PCR and western blot assays. (C,D) Cell proliferation was evaluated by CCK-8 assay after knocking down (C) and overexpressing (D) *ITGB4* in A549 and PC9 cells. (E,F) Effects of *ITGB4* silencing (E) and overexpression (F) on colony formation in LUAD cells. The staining method was crystal violet staining. (G,H) EdU assay was conducted to evaluate LUAD cell proliferation. Cells were stained with Apollo, and DAPI was used to label cell nuclei. Scale bar, 50 μm. Values are expressed as the means ± SDs. *, P<0.05; **, P<0.01; ***, P<0.001. NC, negative control; OE, overexpression; qRT-PCR, quantitative reverse transcription polymerase chain reaction; LUAD, lung adenocarcinoma; CCK-8, Cell Counting Kit-8; SDs, standard deviations.

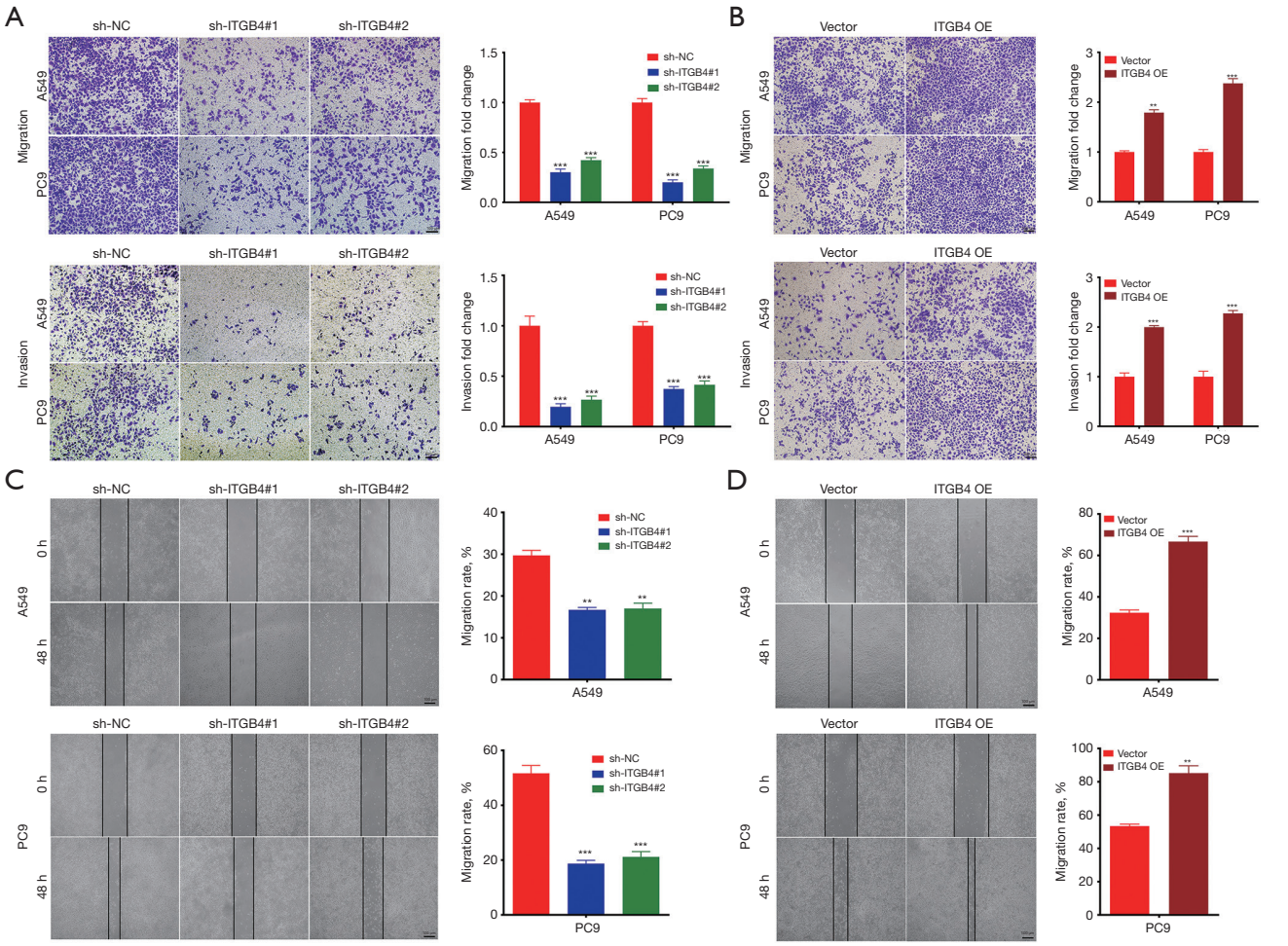

Figure 3 *ITGB4* facilitates LUAD cell migration and invasion *in vitro*. (A) The migration and invasion abilities of cells with *ITGB4* knockdown were evaluated using Transwell assays. The staining method was crystal violet staining. Scale bar, 100 μm. (B) The migration and invasion abilities of cells with *ITGB4* overexpression were assessed. The staining method was crystal violet staining. Scale bar, 100 μm. (C,D) Wound healing assays were conducted to investigate the migratory ability of ITGB4-overexpressing and ITGB4-knockdown LUAD cells. Scale bar, 100 μm. Values are expressed as the means ± SDs. **, P<0.01; ***, P<0.001. NC, negative control; OE, overexpression; LUAD, lung adenocarcinoma; SDs, standard deviations.

genes in ITGB4-silenced cells (Figure S3). KEGG pathway enrichment analysis revealed that these differentially expressed genes were mainly enriched in the *NF-κB* signaling pathway, and a consistent result was observed in TCGA database (*Figure 5A*,*5B*). As expected, *ITGB4* overexpression significantly increased the luciferase activity of *NF-κB*, whereas *ITGB4* knockdown had the opposite effect (*Figure 5C*). Subsequent experiments demonstrated that the phosphorylated levels of proteins such as p-p65, p-IκBα and p-IKKα/β were remarkably increased upon *ITGB4* overexpression but decreased after *ITGB4* silencing. However, the total protein levels of these molecules remained unchanged, except for *IκBα*. Specifically, *ITGB4* overexpression reduced the protein level of *IκBα*, whereas *ITGB4* silencing increased it in LUAD cells (*Figure 5D*). Moreover, *ITGB4* knockdown suppressed the nuclear translocation of *p65* in both A549 and PC9 cells, while *ITGB4* overexpression accelerated the nuclear translocation (*Figure 5E*). These findings indicated that *ITGB4* could activate the *NF-κB* signaling pathway.

To reveal how *ITGB4* promoted the activation of the *NF-κB* signaling, we conducted an IP assay of *ITGB4* with A549 cells, and the IP proteins were subjected to mass spectrometry (Figure S4). Among the proteins identified in

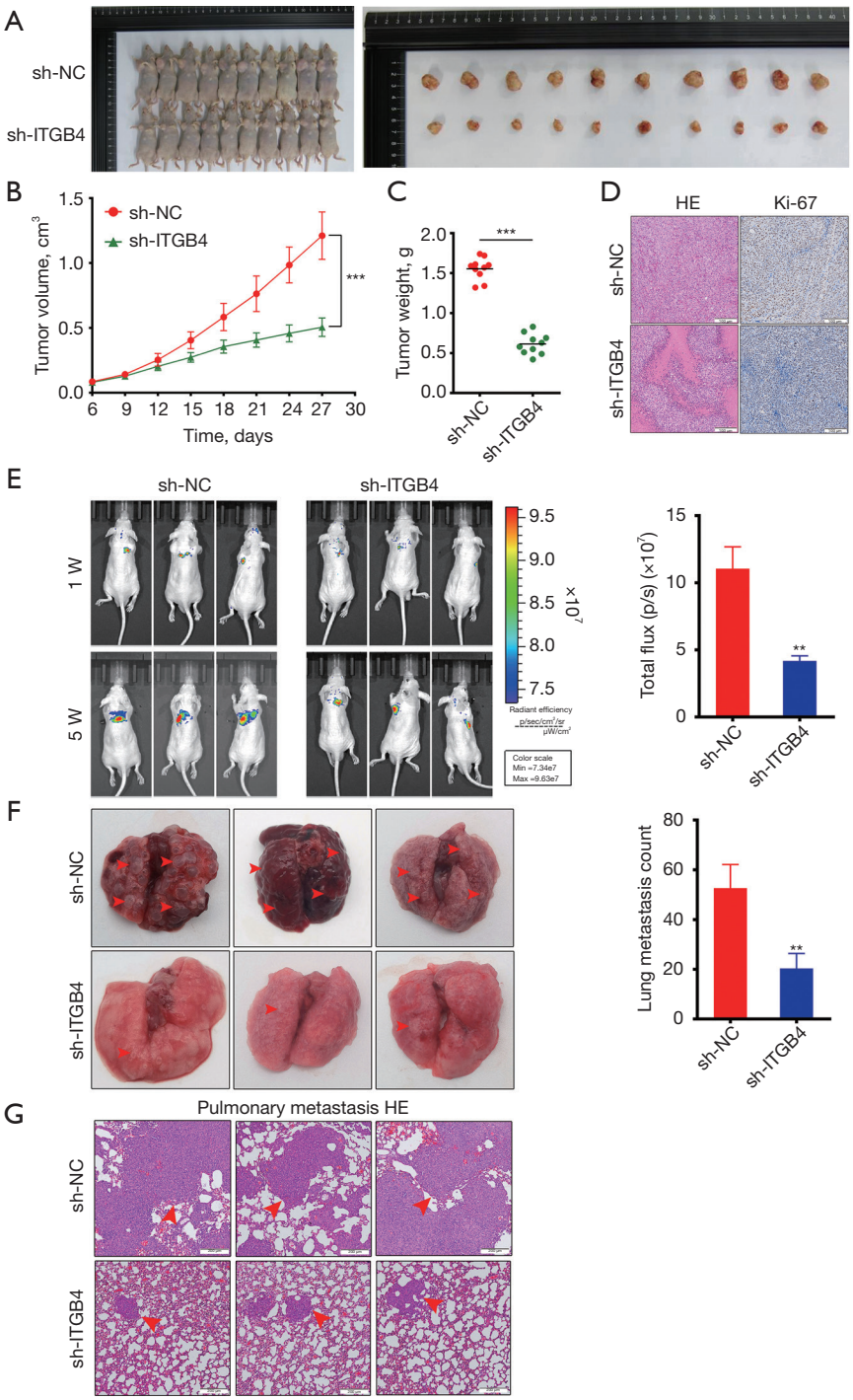

Figure 4 *ITGB4* promotes LUAD cell tumorigenesis and metastasis *in vivo*. (A) Gross appearance of subcutaneous xenograft tumors from the sh-NC and sh-ITGB4 groups (n=10 for each group); (B) tumor volumes were measured every 3 days and the growth curves were calculated; (C) tumor weights were evaluated; (D) HE and Ki-67 IHC staining of xenograft tumors. Scale bar, 100 μm; (E) representative images and histogram analysis of the fluorescence intensity in the lungs after injection of LUAD cells into the tail veins of mice; (F) representative images and histogram analysis of the lung metastatic nodules (arrowheads). (G) HE staining of the lung metastatic nodules (arrowheads). Scale bar, 200 μm. Values are expressed as the means ± SDs. **, P<0.01; ***, P<0.001. NC, negative control; HE, hematoxylin and eosin; LUAD, lung adenocarcinoma; IHC, immunohistochemistry; W, weeks; SDs, standard deviations.

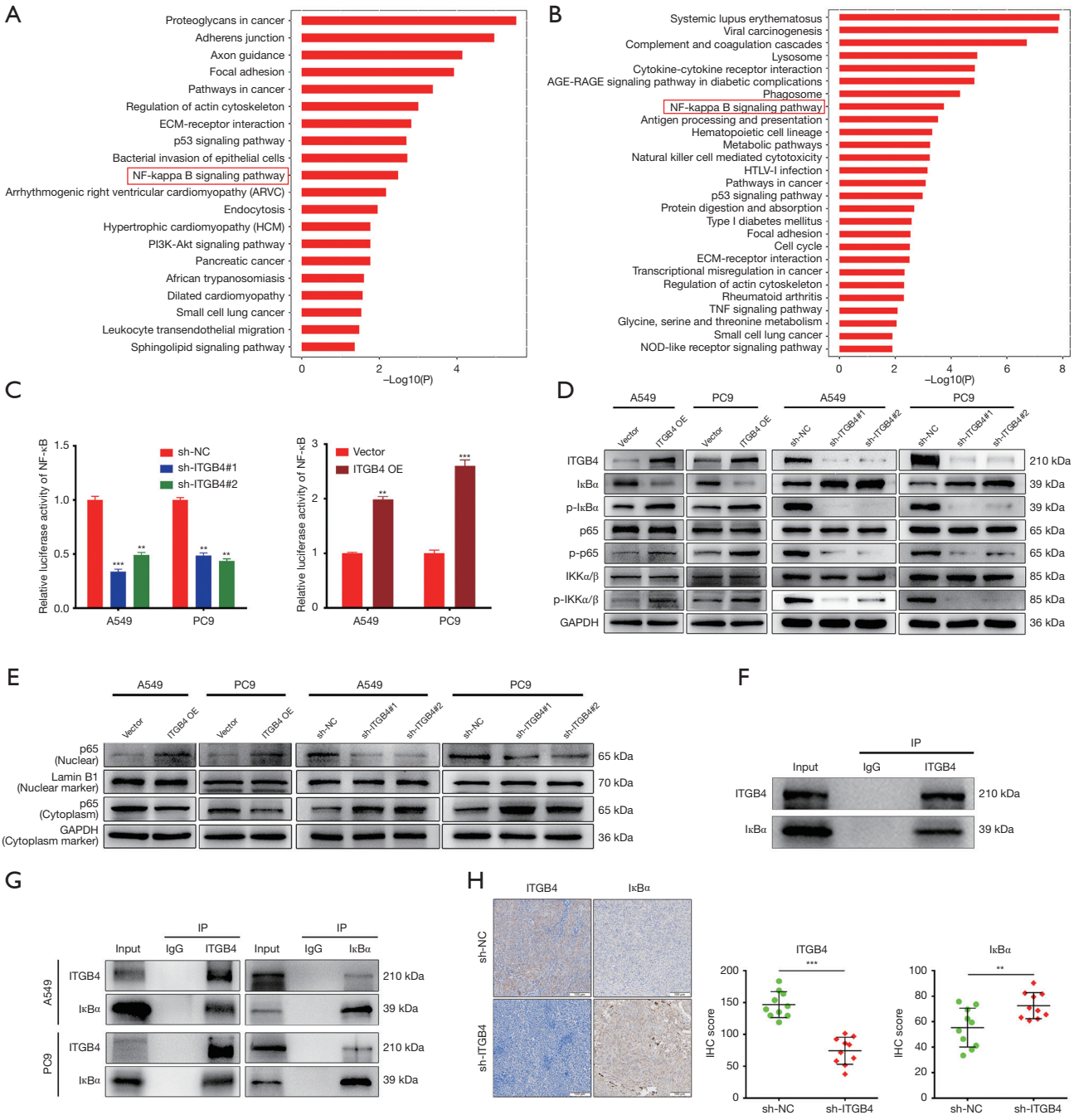

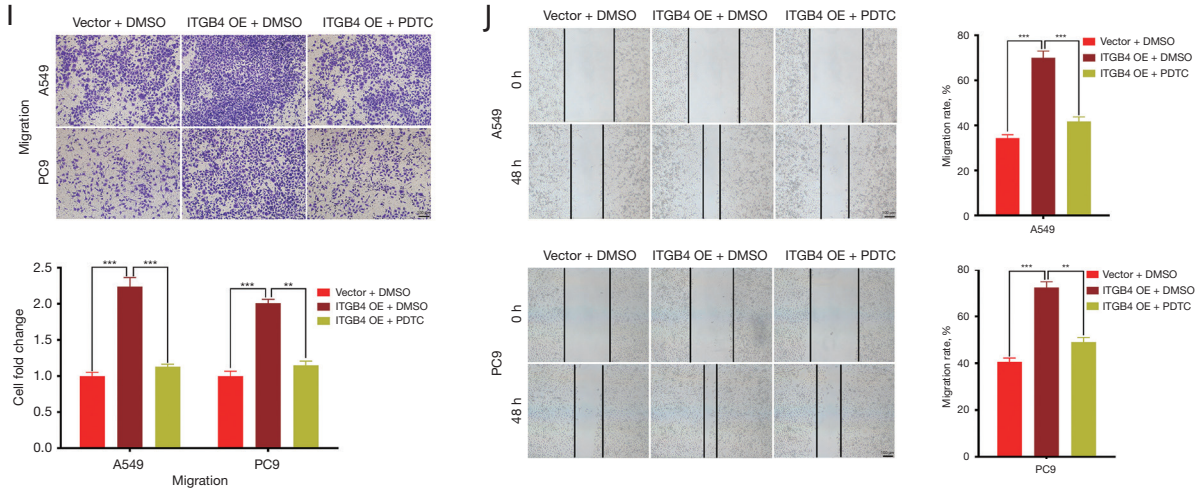

Figure 5 *ITGB4* activates the *NF-κB* signaling pathway by interacting with *IκBα*. (A,B) KEGG pathway enrichment analysis was conducted in TCGA dataset (A) and RNA transcriptome sequencing data (B). (C) The luciferase activity of *NF-κB* was measured after knocking down or overexpressing *ITGB4* in A549 and PC9 cells. (D) Western blot analysis of p-p65, total p65, p-IκBα, total IκBα, p-IKKα/β, and total IKKα/β protein expression in ITGB4-knockdown or ITGB4-overexpressing LUAD cells. (E) Western blot analysis of nuclear and cytoplasmic *p65* protein expression in ITGB4-knockdown or ITGB4-overexpressing LUAD cells. *Lamin B1* was used as a nuclear loading control, while *GAPDH* was used as a cytoplasmic loading control for normalization. (F) Western blot assays were performed on the IP protein (*IκBα*) identified through mass spectrometry in the IP assay of *ITGB4* in A549 cells. (G) The binding of *IκBα* to *ITGB4* in A549 and PC9 cells was detected by co-IP assays. (H) Representative images and histogram analysis of *ITGB4* and *IκBα* IHC analysis in xenograft tumors. The staining method was immunohistochemical staining. Scale bar, 100 μm. (I,J) The cell migration of ITGB4-overexpressing LUAD cells treating with either DMSO or the *NF-κB* inhibitor PDTC was evaluated by Transwell (I) and wound healing (J) assays. The staining method for Transwell assay was crystal violet staining. Scale bar, 100 μm. Values are expressed as the means ± SDs. **, P<0.01; ***, P<0.001. ECM, extracellular matrix; AGE, advanced glycation end product; RAGE, receptor for AGE; HTLV-1, human T-lymphotropic virus type 1; TNF, tumor necrosis factor; NC, negative control; OE, overexpression; IgG, immunoglobulin G; IP, immunoprecipitation; DMSO, dimethyl sulfoxide; PDTC, pyrrolidine dithiocarbamate; LUAD, lung adenocarcinoma; KEGG, Kyoto Encyclopedia of Genes and Genomes; TCGA, The Cancer Genome Atlas; IHC, immunohistochemistry; SDs, standard deviations.

the IP assay (Table S5), we successfully confirmed *IκBα* as the protein that specifically binds to *ITGB4*. From the mass spectrometry data, it was determined that *IκBα* (also referred to as *NFKBIA*) was the sole protein found to be associated with the *NF-κB* signaling pathway. The interaction between *IκBα* and *ITGB4* was validated through western blot analysis (*Figure 5F*). Additionally, co-IP assays demonstrated a direct protein-protein interaction between *ITGB4* and *IκBα* in both A549 and PC9 cells (*Figure 5G*). Moreover, IHC staining performed on xenograft tumors showed an increase in *IκBα* expression upon *ITGB4* silencing (*Figure 5H*). These findings suggested that *ITGB4* could interact with *IκBα* to suppress its expression in LUAD. Previous studies have shown that *IκBα* could limit *p65* transportation into the nucleus and block *NF-κB* signaling (24,25). Therefore, we speculated that *ITGB4* may activate the *NF-κB* signaling pathway through interacting with *IκBα*.

To further explore the role of *NF-κB* signaling in the migration of LUAD cells promoted by *ITGB4*, the classical *NF-κB* inhibitor pyrrolidine dithiocarbamate (PDTC) was used. Transwell and wound healing assays indicated that PDTC significantly inhibited the improved cell migration induced by *ITGB4* overexpression in LUAD cells (*Figure 5I,5J*). These results demonstrated that *NF-κB* signaling may participate in the migratory phenotype induced by *ITGB4* in LUAD.

Laminin-5 enhanced LUAD cell proliferation, migration and invasion through ITGB4 signaling activation

In light of *ITGB4* being a well-known cell surface receptor, we further explored whether its ligand *laminin-5* could activate *ITGB4* signaling and promote LUAD progression. As shown in *Figure 6A*, *laminin-5* stimulation had little

effect on *ITGB4* expression but significantly enhances the activation of the *NF-κB* signaling pathway. Importantly, this stimulatory effect was largely attenuated by *ITGB4* silencing. As expected, *laminin-5* stimulation facilitated LUAD cell proliferation. Furthermore, these proliferative effects could be reversed by knocking down *ITGB4* (*Figure 6B,6C*). Consistently, the transwell assay revealed that *laminin-5* stimulation resulted in a notable increase in the migration and invasion of LUAD cells. Notably, the promotional effects were effectively reversed by *ITGB4* silencing (*Figure 6D,6E*). Similar results were observed in the wound healing assays (*Figure 6F*). These results collectively suggest that *laminin-5*, as an *ITGB4* ligand, could promote LUAD progression by activating *ITGB4* signaling.

ITGB4 suppresses CD4⁺ and CD8⁺ T-cell infiltrations in the TIME of LUAD

According to the GO analysis, *ITGB4* may be involved in various immune-related processes, including the inflammatory response, innate immune response, immune system process, and immune effector process (Figure S5). Therefore, we further investigated whether *ITGB4* could influence T-cell immune responses in LUAD. As shown in *Figure 7A-7C*, LUAD tumors with higher *ITGB4* expression exhibited significantly lower infiltration of $CD4^+$ and $CD8^+$ T cells. To further investigate the effect of *ITGB4* on T-cell infiltrations *in vivo*, an immunocompetent mouse model was established using LLC-sh-ITGB4 cells and C57BL/6J mice. Consistently, *ITGB4* knockdown markedly inhibited the proliferation, migration, and invasion abilities of LLC cells (Figure S6). In the immunocompetent mouse model, mice treated with LLC-sh-ITGB4 cells exhibited significant inhibition of tumor growth (*Figure 7D-7G*). Furthermore, *ITGB4* knockdown increased $CD4^+$ and $CD8^+$ T-cell infiltration in the mouse tumor tissues (*Figure 7H-7K*). Flow cytometric analysis further supported these findings, indicating an elevated population of $CD4^+$ and $CD8^+$ T cells in $CD45^+$ TILs following *ITGB4* silencing (*Figure 7L,7M*). Overall, these findings suggested that *ITGB4* could suppress $CD4^+$ and $CD8^+$ T-cell infiltrations in the TIME of LUAD.

TFAP2A activates the transcription of ITGB4 in LUAD

In order to investigate the potential transcription factors that may activate *ITGB4* transcription in LUAD, we utilized the JASPAR online database (http://jaspar.genereg.net/) and the Animal Transcription Factor Database (http://bioinfo.life.hust.edu.cn/AnimalTFDB#!/). Through this analysis, we predicted 268 transcription factors that have the potential to regulate *ITGB4* expression (*Figure 8A*). Further co-expression analysis based on the TCGA database revealed that 16 of these transcription factors showed a significant correlation with *ITGB4* expression in LUAD ($r \geq 0.3$). Among these transcription factors, *TFAP2A* was found to be aberrantly up-regulated in LUAD and exhibited the strongest correlation with *ITGB4* expression (*Figure 8B,8C*). Moreover, high expression of *TFAP2A* was associated with poorer prognosis according to the TCGA database (*Figure 8D*). Knockdown of *TFAP2A* resulted in a significant reduction in *ITGB4* expression, while overexpression of *TFAP2A* increased *ITGB4* expression (*Figure 8E,8F*). Further investigation revealed that the binding site of *TFAP2A* in the *ITGB4* promoter was located within the region spanning –235 to –222 bp. To validate this, we utilized PCR-mediated mutagenesis to remove the *TFAP2A*-binding motif from the *ITGB4* promoter vector, resulting in a modified construct referred to as ITGB4-MUT. The original, unmodified construct was denoted as ITGB4-WT (*Figure 8G*). Furthermore, it was observed that *TFAP2A* overexpression significantly enhanced luciferase activity in the ITGB4-WT group, whereas *TFAP2A* knockdown resulted in a decrease in luciferase activity. Importantly, the luciferase activity of the ITGB4-MUT group remained unaffected by *TFAP2A* modulation (*Figure 8H*). ChIP assay also revealed that DNA fragments containing the putative *TFAP2A*-binding site were enriched in the chromatin immunoprecipitated by the anti-TFAP2A antibody compared with the control (anti-IgG) (*Figure 8I*). These findings indicated that *TFAP2A* could activate *ITGB4* transcription by directly binding to the *ITGB4* promoter in LUAD cells. The schematic diagram of this study was shown in *Figure 8J*.

Discussion

Immune-related genes play a crucial role in regulating tumor progression and immune responses in various types of malignant tumors, including LUAD. For instance, the immune-related gene *FSCN1* is associated with the infiltration of $CD4^+$ T cells, thereby promoting the development of LUAD (26). *DFNA5* could regulate T cell exhaustion and influence the prognosis of patients with LUAD (27). Consistent with previous findings, the present study has unveiled a novel immune-associated gene, *ITGB4*,

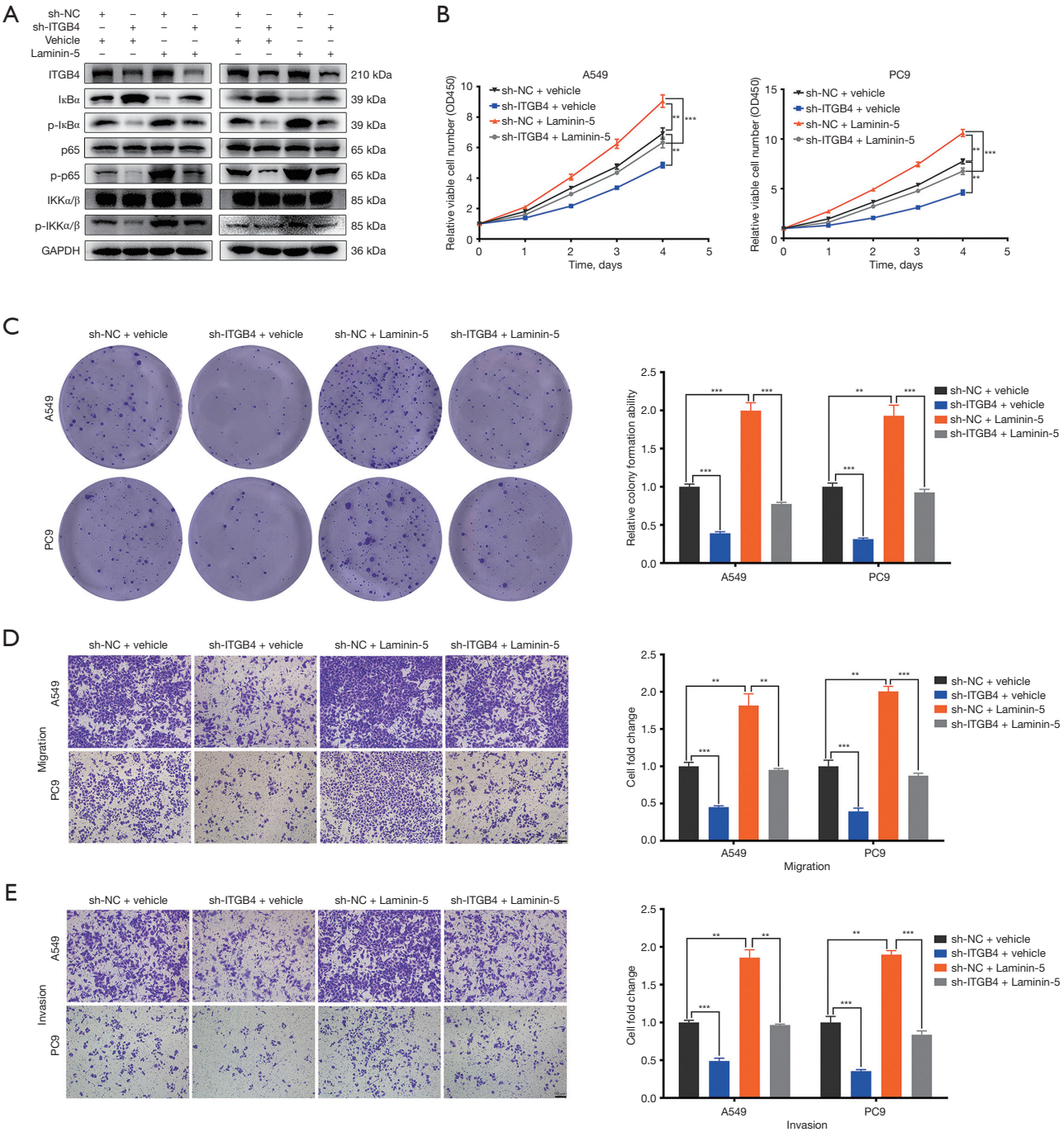
A
sh-NC
sh-ITGB4
Vehicle
Laminin-5
ITGB4
IκBα
p-IκBα
p65
p-p65
IKKα/β
p-IKKα/β
GAPDH
210 kDa
39 kDa
39 kDa
65 kDa
65 kDa
85 kDa
85 kDa
36 kDa
B
A549
PC9
sh-NC + vehicle
sh-ITGB4 + vehicle
sh-NC + Laminin-5
sh-ITGB4 + Laminin-5
Relative viable cell number (OD450)
Time, days
C
sh-NC + vehicle
sh-ITGB4 + vehicle
sh-NC + Laminin-5
sh-ITGB4 + Laminin-5
A549
PC9
Relative colony formation ability
D
Migration
Cell fold change
E
Invasion

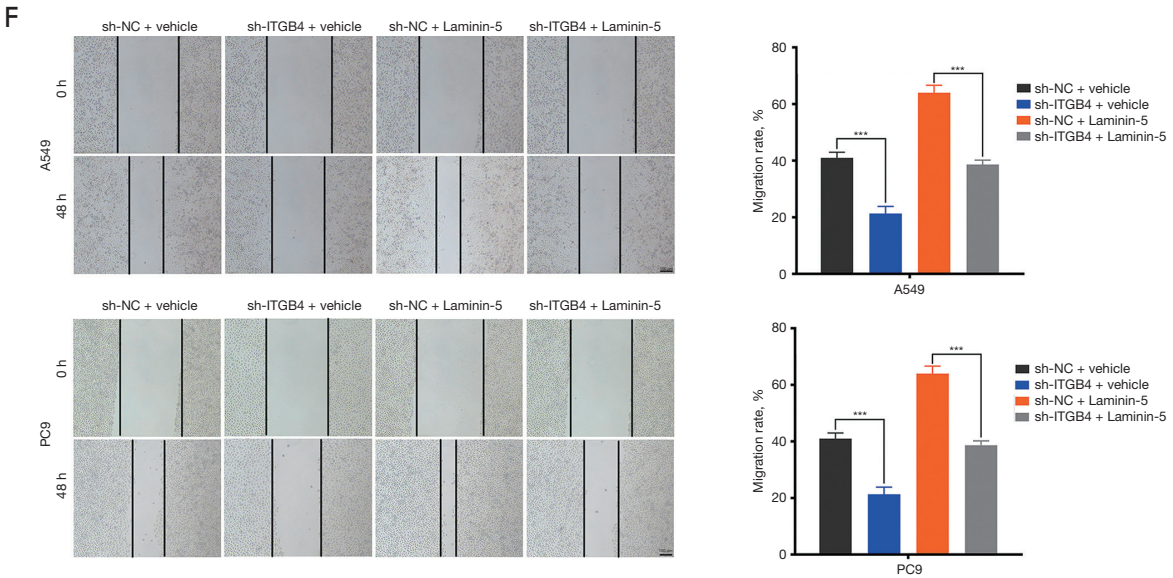

Figure 6 *Laminin-5* promotes LUAD cell proliferation, migration and invasion through *ITGB4* signaling activation. (A) Western blot analysis of p-IκBα, total *IκBα*, p-p65, total *p65*, p-IKKα/β, and total IKKα/β protein expression in sh-NC or sh-ITGB4 LUAD cells, both in the presence or absence of 10 ng/mL recombinant *laminin-5* protein. (B) CCK-8 assay was performed with sh-NC or sh-ITGB4 LUAD cells in the presence or absence of recombinant *laminin-5*. (C) Colony formation assay was conducted to evaluate cell proliferation in sh-NC or sh-ITGB4 LUAD cells treated with or without *laminin-5*. The staining method was crystal violet staining. (D,E) Transwell assays were performed to assess the migration (D) and invasion (E) capabilities of sh-NC or sh-ITGB4 LUAD cells treated with or without *laminin-5*. The staining method was crystal violet staining. Scale bar, 100 μm. (F) Wound healing assay was carried out to evaluate cell migration in sh-NC or sh-ITGB4 LUAD cells treated with or without *laminin-5*. Scale bar, 100 μm. Values are expressed as the means ± SDs. **, P<0.01; ***, P<0.001. CCK-8, Cell Counting Kit-8; NC, negative control; LUAD, lung adenocarcinoma; SDs, standard deviations.

which could promote LUAD progression and inhibit $CD4^+$/$CD8^+$ T-cell infiltrations.

ITGB4, a crucial member of the integrin family, plays a critical role in cell migration, adhesion and differentiation in cancers (22,28,29). Upregulation of *ITGB4* has been observed in various malignant tumors, including glioma, gastric and cervical cancer (30-32). In lung cancer, aberrant *ITGB4* expression is associated with decreased overall survival (23,33). Activation of *ITGB4* signaling by *KCNF1* has been reported to be involved in accelerating the progression of lung cancer (34). However, the specific functions and underlying mechanisms of *ITGB4* in LUAD progression are yet to be fully elucidated. Consistent with previous findings, the present study revealed that patients with higher *ITGB4* expression had a worse prognosis. Moreover, functional assays indicated that *ITGB4* could promote LUAD progression *in vitro* and *in vivo*.

Previous studies have shown that *IκBα* could limit *p65* transportation into the nucleus and block *NF-κB* signaling. However, upon phosphorylation by the activated IκB kinase complex, *IκBα* is degraded, resulting in the activation of *NF-κB* (24, 25). Indeed, activation of the *NF-κB* signaling has been extensively reported to promote the progression of lung cancer (35-37). Consistent with these observations, our study revealed that *ITGB4* could activate the *NF-κB* signaling through interacting with *IκBα* in LUAD. Moreover, functional assays indicated that *NF-κB* signaling may participate in the migratory phenotype induced by *ITGB4*. However, the precise interaction between *ITGB4* and *IκBα*, including the specific binding domain, remains unclear. This represents a limitation in our current research, and we intend to conduct further exploration in future studies. Additionally, it is noteworthy that *ITGB4* could serve as a cell surface receptor for various ligands. Among them, *laminin-5* has been identified as a structural ligand that binds to *ITGB4*, thereby promoting tumor migration and invasion (38,39). Indeed, our results also suggested that *laminin-5* could promote LUAD progression by activating the *ITGB4* signaling.

The *NF-κB* signaling pathway plays a crucial role in

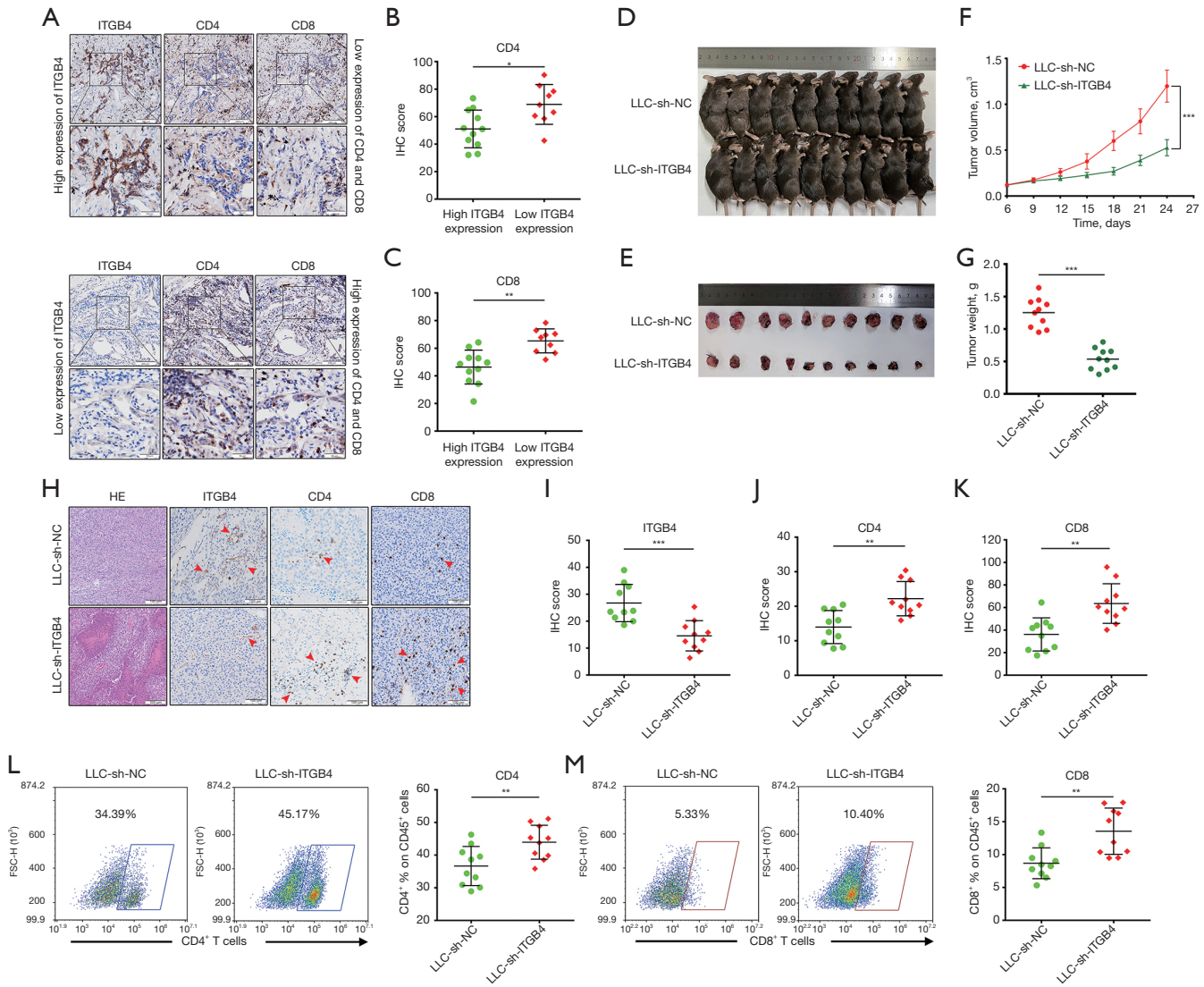

Figure 7 *ITGB4* suppresses CD4$^+$ and CD8$^+$ T-cell infiltrations in the tumor immune microenvironment of LUAD. (A) Representative images of *ITGB4*, CD4 and CD8 IHC analysis in LUAD tumor tissues from 20 patients. Scale bars, 200 and 50 μm. (B,C) Correlation between *ITGB4* and CD4 (B), CD8 (C) IHC scores of 20 LUAD samples. (D-G) An immunocompetent mouse model was established by injecting LLC-sh-NC or LLC-sh-ITGB4 cells into the right flanks of C57BL/6J mice: (D,E) gross appearance of subcutaneous tumors from the LLC-sh-NC or LLC-sh-ITGB4 groups (n=10 for each group); (F) tumor volumes were measured every 3 days and growth curves were calculated; (G) tumor weights were evaluated. (H-K) HE and IHC staining of tumors from the immunocompetent mouse model: (H) representative images of IHC staining for *ITGB4*, CD4 and CD8 in tumors from the LLC-sh-NC or LLC-sh-ITGB4 groups. Red arrowheads indicated the positive area. Scale bar, 100 μm; (I-K) IHC scores of *ITGB4* (I), CD4 (J) and CD8 (K) protein expression were analyzed. (L,M) The populations of CD4$^+$ (L) and CD8$^+$ (M) T cells in CD45$^+$ TILs in tumors from LLC-sh-NC or LLC-sh-ITGB4 group were analyzed by flow cytometry. Values are expressed as the means ± SDs. *, P<0.05; **, P<0.01; ***, P<0.001. NC, negative control; LLC, Lewis lung carcinoma; HE, hematoxylin and eosin; IHC, immunohistochemistry; FSC-H, forward scatter-height; LUAD, lung adenocarcinoma; SDs, standard deviations.

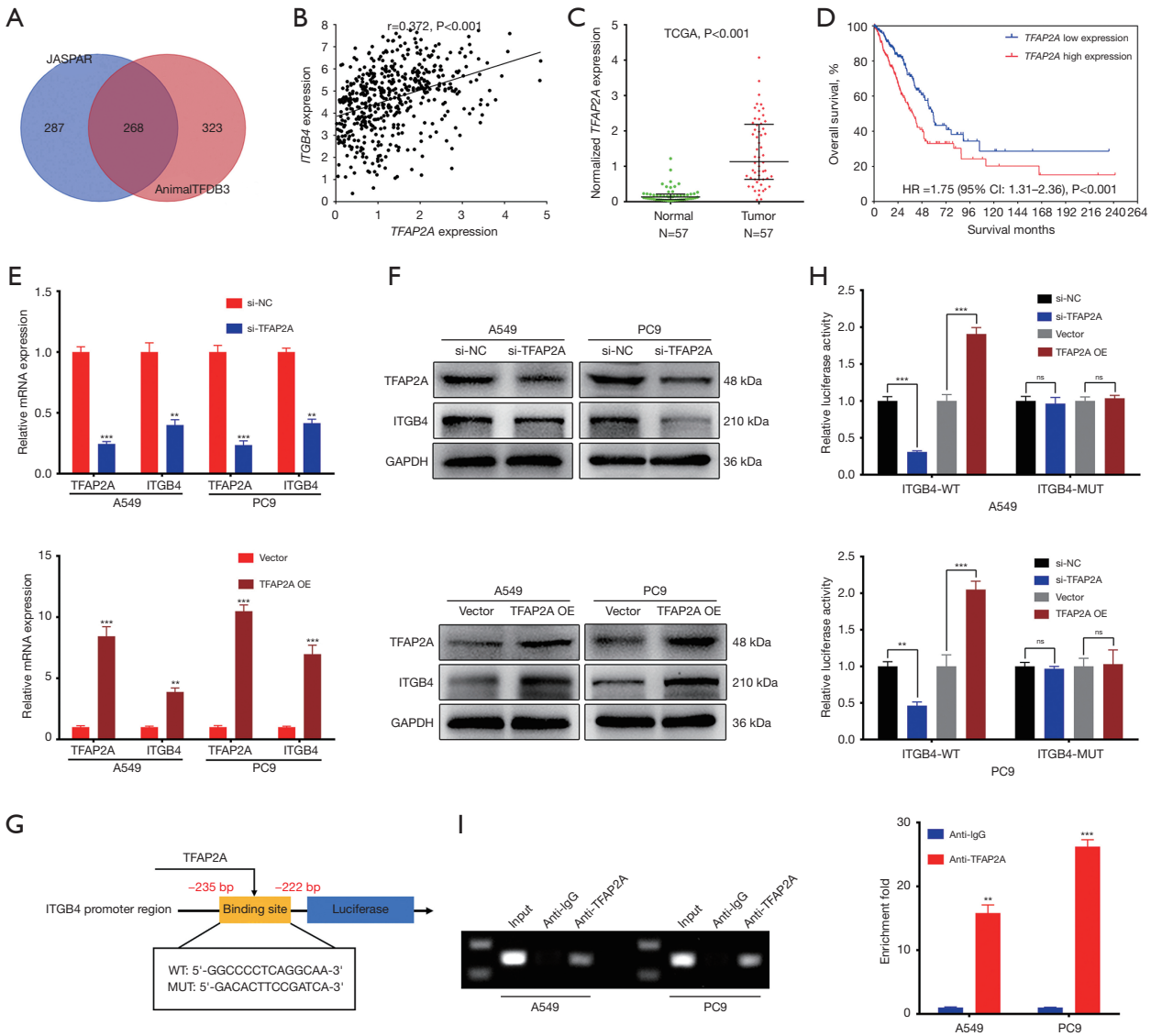
A
JASPAR
287
268
323
AnimalTFDB3
B
r=0.372, P<0.001
ITGB4 expression
TFAP2A expression
C
TCGA, P<0.001
Normalized TFAP2A expression
Normal N=57
Tumor N=57
D
TFAP2A low expression
TFAP2A high expression
Overall survival, %
HR =1.75 (95% CI: 1.31–2.36), P<0.001
Survival months
E
si-NC
si-TFAP2A
Relative mRNA expression
TFAP2A
ITGB4
A549
PC9
Vector
TFAP2A OE
F
A549
PC9
si-NC
si-TFAP2A
Vector
TFAP2A OE
TFAP2A
ITGB4
GAPDH
48 kDa
210 kDa
36 kDa
H
Relative luciferase activity
ITGB4-WT
ITGB4-MUT
ns
G
TFAP2A
−235 bp
−222 bp
ITGB4 promoter region
Binding site
Luciferase
WT: 5'-GGCCCCTCAGGCAA-3'
MUT: 5'-GACACTTCCGATCA-3'
I
Input
Anti-IgG
Anti-TFAP2A
Anti-IgG
Anti-TFAP2A
Enrichment fold

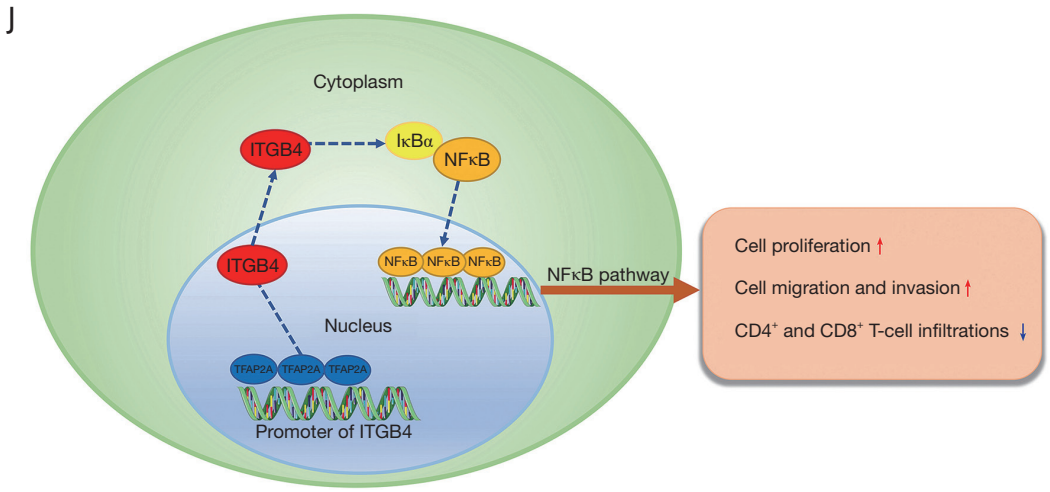

Figure 8 *TFAP2A* activates the transcription of *ITGB4* in LUAD cells. (A) The JASPAR and AnimalTFDB3 databases were used to predict the transcription factor that activated *ITGB4* transcription in LUAD cells. (B) Correlation between *TFAP2A* and *ITGB4* expression was evaluated by co-expression analysis based on TCGA database. (C) *TFAP2A* was significantly up-regulated in LUAD compared with adjacent normal tissues in TCGA database. (D) LUAD patients with a higher *TFAP2A* expression had a worse prognosis in TCGA dataset. (E,F) Relative mRNA (E) and protein (F) levels of *ITGB4* after *TFAP2A* knockdown or overexpression in A549 and PC9 cells. (G) The binding site of *TFAP2A* in the *ITGB4* promoter was at the region –235 to –222 bp. The *ITGB4* promoter was cloned into the pGL3-basic luciferase vector (pGL3-ITGB4 wild-type, named ITGB4-WT), while the *TFAP2A*-binding motif was removed from the *ITGB4* promoter vector (pGL3-ITGB4 mutant, named ITGB4-MUT). (H) Dual-luciferase reporter assay was performed to evaluate the effect of *TFAP2A* on the activity of ITGB4-WT and ITGB4-MUT. (I) ChIP qPCR analyses were performed to evaluate the enrichment of the DNA fragment containing the putative *TFAP2A*-binding site in the chromatin that was precipitated by the anti-TFAP2A antibody. Anti-IgG antibody was used as a negative control. (J) Schematic diagram illustrating the molecular mechanism by which *ITGB4* promoted LUAD progression and suppressed $CD4^+$/$CD8^+$ T-cell infiltrations. The red arrows represent enhanced cell proliferation, migration, and invasion, while the blue arrows indicate reduced infiltration of $CD4^+$ and $CD8^+$ T cells. Values are expressed as the means ± SDs. **, P<0.01; ***, P<0.001. ns, not significant; TCGA, The Cancer Genome Atlas; HR, hazard ratio; NC, negative control; IgG, immunoglobulin G; LUAD, lung adenocarcinoma; ChIP, Chromatin immunoprecipitation; SDs, standard deviations; qPCR, quantitative polymerase chain reaction.

mediating T-cell immune responses and influencing $CD4^+$/$CD8^+$ T-cell infiltration (40,41). Notably, *IκBα* could also promote $CD8^+$ T-cell immunity in tumors (42). In our study, we discovered a negative correlation between *ITGB4* expression and the infiltration of $CD4^+$ and $CD8^+$ T cells in LUAD. This finding is consistent with previous studies reporting the involvement of *ITGB4* in immune responses. For example, Tang *et al.* demonstrated that deficiency in airway epithelial *ITGB4* in early life enhanced allergic immune responses (21). In LUAD, *ITGB4* was reported to be positively associated with the infiltration of $CD4^+$ T cells. Moreover, *ITGB4* may affect immune cell infiltration through influencing immunomodulation-related genes (33). Indeed, increased infiltrations of $CD4^+$ and $CD8^+$ T lymphocytes were correlated with improved prognosis in patients with LUAD (43,44). Based on these findings, we hypothesized that *ITGB4* might inhibit $CD4^+$/$CD8^+$ T-cell infiltrations through suppressing *IκBα* expression to activate the *NF-κB* signaling. However, the specific mechanism requires further in-depth research in the future.

In the current study, a significant suppression of LUAD cell tumorigenesis and metastasis *in vivo* was observed following *ITGB4* knockdown. Remarkably, Ruan *et al.* indicated that ITGB4-targeted immunotherapies could effectively suppress tumor growth and reduce metastasis in various malignancies. Notably, the efficacy of ITGB4-targeted immunotherapies is significantly enhanced when combined with anti-PD-L1 treatment (45). *PD-L1* can directly bind to *ITGB4* to facilitate tumor progression and is able to hinder antitumor immunity by diminishing the infiltration of T lymphocytes, particularly $CD8^+$ T cells (32,46,47). These findings suggested that *ITGB4* might have

potential to influence the outcomes of anti-PD-1/PD-L1 immunotherapies and serve as a novel immunotherapeutic target for the treatment of LUAD. However, a limitation of our study is that we did not experimentally investigate the specific impact of *ITGB4* in lung adenocarcinoma on anti-PD-1/PD-L1 immunotherapies, which is a focus of our future research efforts.

Our study revealed that *TFAP2A* can activate *ITGB4* transcription in LUAD by directly binding to the *ITGB4* promoter. The association between *TFAP2A* and *ITGB4* expression has also been reported in pancreatic and colorectal cancer, although these findings have not been validated by functional assays (48,49). Importantly, *TFAP2A* has been implicated in promoting tumor progression in LUAD through the transcriptional regulation of other oncogenes. For instance, *TFAP2A* transcriptionally activates *PSG9*, leading to accelerated tumor progression in LUAD (50). Additionally, *TFAP2A* facilitates LUAD metastasis by positively regulating the transcription of *ITPKA* (51). Furthermore, significant bioinformatics research has uncovered similar biomarkers that could complement the present findings in this study. For instance, investigators have identified *FEN1* as a facilitator of hepatocellular carcinoma progression through the enhancement of *USP7*/*MDM2*-mediated *P53* inactivation (52). Additionally, researchers have demonstrated the chaperone function of *HSP90-CDC37* in the oncogenic *FGFR3-TACC3* fusion (53). These studies provide robust support for our findings.

Conclusions

ITGB4 was transcriptionally activated by *TFAP2A*, and could promote LUAD progression and suppress $CD4^+$/$CD8^+$ T-cell infiltrations by targeting the *NF-κB* signaling pathway. Therefore, *ITGB4* may be a potential novel prognostic biomarker and a promising immunotherapeutic target for LUAD.

Acknowledgments

We thank the study participants and research staff for their contributions to this study.

Funding: This work was supported by the National Natural Science Foundation of China (Nos. 82203296 and 82303458), and the Young Scholars Fostering Fund of The First Affiliated Hospital of Nanjing Medical University (No. PY2021024).

Footnote

Reporting Checklist: The authors have completed the MDAR reporting checklist. Available at https://tlcr.amegroups.com/article/view/10.21037/tlcr-24-50/rc

Data Sharing Statement: Available at https://tlcr.amegroups.com/article/view/10.21037/tlcr-24-50/dss

Peer Review File: Available at https://tlcr.amegroups.com/article/view/10.21037/tlcr-24-50/prf

Conflicts of Interest: All authors have completed the ICMJE uniform disclosure form (available at https://tlcr.amegroups.com/article/view/10.21037/tlcr-24-50/coif). The authors have no conflicts of interest to declare.

Ethical Statement: The authors are accountable for all aspects of the work in ensuring that questions related to the accuracy or integrity of any part of the work are appropriately investigated and resolved. Written informed consent was obtained from all individual participants. All the procedures involving patient samples were compliant with all relevant ethical regulations and approved by the Research Ethics Committee of The First Affiliated Hospital of Nanjing Medical University (Approval No. 2019-SR-123). The study was conducted in accordance with the Declaration of Helsinki (as revised in 2013). And all animal experiments were performed under a project license (Approval No. IACUC-2208008) granted by the Ethics Committee of Nanjing Medical University, in compliance with the guidelines of the Ethics Committee of Nanjing Medical University for the care and use of animals.

References

1. Sung H, Ferlay J, Siegel RL, et al. Global Cancer Statistics 2020: GLOBOCAN Estimates of Incidence and Mortality

Worldwide for 36 Cancers in 185 Countries. CA Cancer J Clin 2021;71:209-49.
2. Ettinger DS, Wood DE, Akerley W, et al. Non-Small Cell Lung Cancer, Version 6.2015. J Natl Compr Canc Netw 2015;13:515-24.
3. Yang L, He YT, Dong S, et al. Single-cell transcriptome analysis revealed a suppressive tumor immune microenvironment in EGFR mutant lung adenocarcinoma. J Immunother Cancer 2022;10:e003534.
4. Zavitsanou AM, Pillai R, Hao Y, et al. KEAP1 mutation in lung adenocarcinoma promotes immune evasion and immunotherapy resistance. Cell Rep 2023;42:113295.
5. Remark R, Becker C, Gomez JE, et al. The non-small cell lung cancer immune contexture. A major determinant of tumor characteristics and patient outcome. Am J Respir Crit Care Med 2015;191:377-90.
6. Lambrechts D, Wauters E, Boeckx B, et al. Phenotype molding of stromal cells in the lung tumor microenvironment. Nat Med 2018;24:1277-89.
7. Thommen DS, Koelzer VH, Herzig P, et al. A transcriptionally and functionally distinct PD-1(+) CD8(+) T cell pool with predictive potential in non-small-cell lung cancer treated with PD-1 blockade. Nat Med 2018;24:994-1004.
8. Johnson SK, Kerr KM, Chapman AD, et al. Immune cell infiltrates and prognosis in primary carcinoma of the lung. Lung Cancer 2000;27:27-35.
9. Hiraoka K, Miyamoto M, Cho Y, et al. Concurrent infiltration by CD8+ T cells and CD4+ T cells is a favourable prognostic factor in non-small-cell lung carcinoma. Br J Cancer 2006;94:275-80.
10. Ruffini E, Asioli S, Filosso PL, et al. Clinical significance of tumor-infiltrating lymphocytes in lung neoplasms. Ann Thorac Surg 2009;87:365-71; discussion 371-2.
11. Kawai O, Ishii G, Kubota K, et al. Predominant infiltration of macrophages and CD8(+) T Cells in cancer nests is a significant predictor of survival in stage IV nonsmall cell lung cancer. Cancer 2008;113:1387-95.
12. Goc J, Germain C, Vo-Bourgais TK, et al. Dendritic cells in tumor-associated tertiary lymphoid structures signal a Th1 cytotoxic immune contexture and license the positive prognostic value of infiltrating CD8+ T cells. Cancer Res 2014;74:705-15.
13. Kinoshita F, Tagawa T, Akamine T, et al. Interleukin-38 promotes tumor growth through regulation of CD8(+) tumor-infiltrating lymphocytes in lung cancer tumor microenvironment. Cancer Immunol Immunother 2021;70:123-35.
14. Yarchoan M, Hopkins A, Jaffee EM. Tumor Mutational Burden and Response Rate to PD-1 Inhibition. N Engl J Med 2017;377:2500-1.
15. Schoenfeld AJ, Arbour KC, Rizvi H, et al. Severe immune-related adverse events are common with sequential PD-(L)1 blockade and osimertinib. Ann Oncol 2019;30:839-44.
16. Cesano A. nCounter(®) PanCancer Immune Profiling Panel (NanoString Technologies, Inc., Seattle, WA). J Immunother Cancer 2015;3:42.
17. Lu F, Zhao Y, Pang Y, et al. NLRP3 inflammasome upregulates PD-L1 expression and contributes to immune suppression in lymphoma. Cancer Lett 2021;497:178-89.
18. Ma S, Cheng Q, Cai Y, et al. IL-17A produced by γδ T cells promotes tumor growth in hepatocellular carcinoma. Cancer Res 2014;74:1969-82.
19. Tosti N, Cremonesi E, Governa V, et al. Infiltration by IL22-Producing T Cells Promotes Neutrophil Recruitment and Predicts Favorable Clinical Outcome in Human Colorectal Cancer. Cancer Immunol Res 2020;8:1452-62.
20. Jiao X, Sherman BT, Huang da W, et al. DAVID-WS: a stateful web service to facilitate gene/protein list analysis. Bioinformatics 2012;28:1805-6.
21. Tang S, Du X, Yuan L, et al. Airway epithelial ITGB4 deficiency in early life mediates pulmonary spontaneous inflammation and enhanced allergic immune response. J Cell Mol Med 2020;24:2761-71.
22. Yuan L, Du X, Tang S, et al. ITGB4 deficiency induces senescence of airway epithelial cells through p53 activation. FEBS J 2019;286:1191-203.
23. Chen Z, Yang X, Bi G, et al. Ligand-receptor interaction atlas within and between tumor cells and T cells in lung adenocarcinoma. Int J Biol Sci 2020;16:2205-19.
24. Zhang L, Zhang K, Zhang J, et al. Loss of fragile site-associated tumor suppressor promotes antitumor immunity via macrophage polarization. Nat Commun 2021;12:4300.
25. Ji J, Ding K, Luo T, et al. TRIM22 activates NF-κB signaling in glioblastoma by accelerating the degradation of IκBα. Cell Death Differ 2021;28:367-81.
26. Shi Y, Xu Y, Xu Z, et al. TKI resistant-based prognostic immune related gene signature in LUAD, in which FSCN1 contributes to tumor progression. Cancer Lett 2022;532:215583.
27. Hu J, Pei W, Jiang M, et al. DFNA5 regulates immune cells infiltration and exhaustion. Cancer Cell Int

2022;22:107.
28. Sung JS, Kang CW, Kang S, et al. ITGB4-mediated metabolic reprogramming of cancer-associated fibroblasts. Oncogene 2020;39:664-76.
29. Han L, Wang L, Tang S, et al. ITGB4 deficiency in bronchial epithelial cells directs airway inflammation and bipolar disorder-related behavior. J Neuroinflammation 2018;15:246.
30. Hong D, Zhang X, Li R, et al. Deletion of TMEM268 inhibits growth of gastric cancer cells by downregulating the ITGB4 signaling pathway. Cell Death Differ 2019;26:1453-66.
31. Ma B, Zhang L, Zou Y, et al. Reciprocal regulation of integrin β4 and KLF4 promotes gliomagenesis through maintaining cancer stem cell traits. J Exp Clin Cancer Res 2019;38:23.
32. Wang S, Li J, Xie J, et al. Programmed death ligand 1 promotes lymph node metastasis and glucose metabolism in cervical cancer by activating integrin β4/SNAI1/SIRT3 signaling pathway. Oncogene 2018;37:4164-80.
33. Wu J, Wang W, Li Z, et al. The prognostic and immune infiltration role of ITGB superfamily members in non-small cell lung cancer. Am J Transl Res 2022;14:6445-66.
34. Chen CY, Wu PY, Van Scoyk M, et al. KCNF1 promotes lung cancer by modulating ITGB4 expression. Cancer Gene Ther 2023;30:414-23.
35. El-Nikhely N, Karger A, Sarode P, et al. Metastasis-Associated Protein 2 Represses NF-κB to Reduce Lung Tumor Growth and Inflammation. Cancer Res 2020;80:4199-211.
36. Ren Y, Cao L, Wang L, et al. Autophagic secretion of HMGB1 from cancer-associated fibroblasts promotes metastatic potential of non-small cell lung cancer cells via NFκB signaling. Cell Death Dis 2021;12:858.
37. Dimitrakopoulos FD, Kottorou AE, Kalofonou M, et al. The Fire Within: NF-κB Involvement in Non-Small Cell Lung Cancer. Cancer Res 2020;80:4025-36.
38. Rousselle P, Scoazec JY. Laminin 332 in cancer: When the extracellular matrix turns signals from cell anchorage to cell movement. Semin Cancer Biol 2020;62:149-65.
39. Schinke H, Shi E, Lin Z, et al. A transcriptomic map of EGFR-induced epithelial-to-mesenchymal transition identifies prognostic and therapeutic targets for head and neck cancer. Mol Cancer 2022;21:178.
40. Hopewell EL, Zhao W, Fulp WJ, et al. Lung tumor NF-κB signaling promotes T cell-mediated immune surveillance. J Clin Invest 2013;123:2509-22.
41. Li L, Han L, Sun F, et al. NF-κB RelA renders tumor-associated macrophages resistant to and capable of directly suppressing CD8(+) T cells for tumor promotion. Oncoimmunology 2018;7:e1435250.
42. Lisiero DN, Cheng Z, Tejera MM, et al. IκBα Nuclear Export Enables 4-1BB-Induced cRel Activation and IL-2 Production to Promote CD8 T Cell Immunity. J Immunol 2020;205:1540-53.
43. Peng H, Wu X, Zhong R, et al. Profiling Tumor Immune Microenvironment of Non-Small Cell Lung Cancer Using Multiplex Immunofluorescence. Front Immunol 2021;12:750046.
44. Edlund K, Madjar K, Mattsson JSM, et al. Prognostic Impact of Tumor Cell Programmed Death Ligand 1 Expression and Immune Cell Infiltration in NSCLC. J Thorac Oncol 2019;14:628-40.
45. Ruan S, Lin M, Zhu Y, et al. Integrin β4-Targeted Cancer Immunotherapies Inhibit Tumor Growth and Decrease Metastasis. Cancer Res 2020;80:771-83.
46. Juneja VR, McGuire KA, Manguso RT, et al. PD-L1 on tumor cells is sufficient for immune evasion in immunogenic tumors and inhibits CD8 T cell cytotoxicity. J Exp Med 2017;214:895-904.
47. Peng Q, Qiu X, Zhang Z, et al. PD-L1 on dendritic cells attenuates T cell activation and regulates response to immune checkpoint blockade. Nat Commun 2020;11:4835.
48. Zhuang H, Zhou Z, Ma Z, et al. Characterization of the prognostic and oncologic values of ITGB superfamily members in pancreatic cancer. J Cell Mol Med 2020;24:13481-93.
49. Mao X, Zhang X, Zheng X, et al. Curcumin suppresses LGR5(+) colorectal cancer stem cells by inducing autophagy and via repressing TFAP2A-mediated ECM pathway. J Nat Med 2021;75:590-601.
50. Xiong Y, Feng Y, Zhao J, et al. TFAP2A potentiates lung adenocarcinoma metastasis by a novel miR-16 family/TFAP2A/PSG9/TGF-β signaling pathway. Cell Death Dis 2021;12:352.
51. Guoren Z, Zhaohui F, Wei Z, et al. TFAP2A Induced ITPKA Serves as an Oncogene and Interacts with DBN1 in Lung Adenocarcinoma. Int J Biol Sci 2020;16:504-14.
52. Bian S, Ni W, Zhu M, et al. Flap endonuclease 1 Facilitated Hepatocellular Carcinoma Progression by

Enhancing USP7/MDM2-mediated P53 Inactivation. Int J Biol Sci 2022;18:1022-38.
53. Li T, Mehraein-Ghomi F, Forbes ME, et al. HSP90-CDC37 functions as a chaperone for the oncogenic FGFR3-TACC3 fusion. Mol Ther 2022;30:1610-27.

Cite this article as: Pan C, Wang Z, Wang Q, Wang H, Deng X, Chen L, Li Z. *TFAP2A*-activated *ITGB4* promotes lung adenocarcinoma progression and inhibits $CD4^+$/$CD8^+$ T-cell infiltrations by targeting *NF-κB* signaling pathway. Transl Lung Cancer Res 2024;13(9):2116-2138. doi: 10.21037/tlcr-24-50

Supplementary

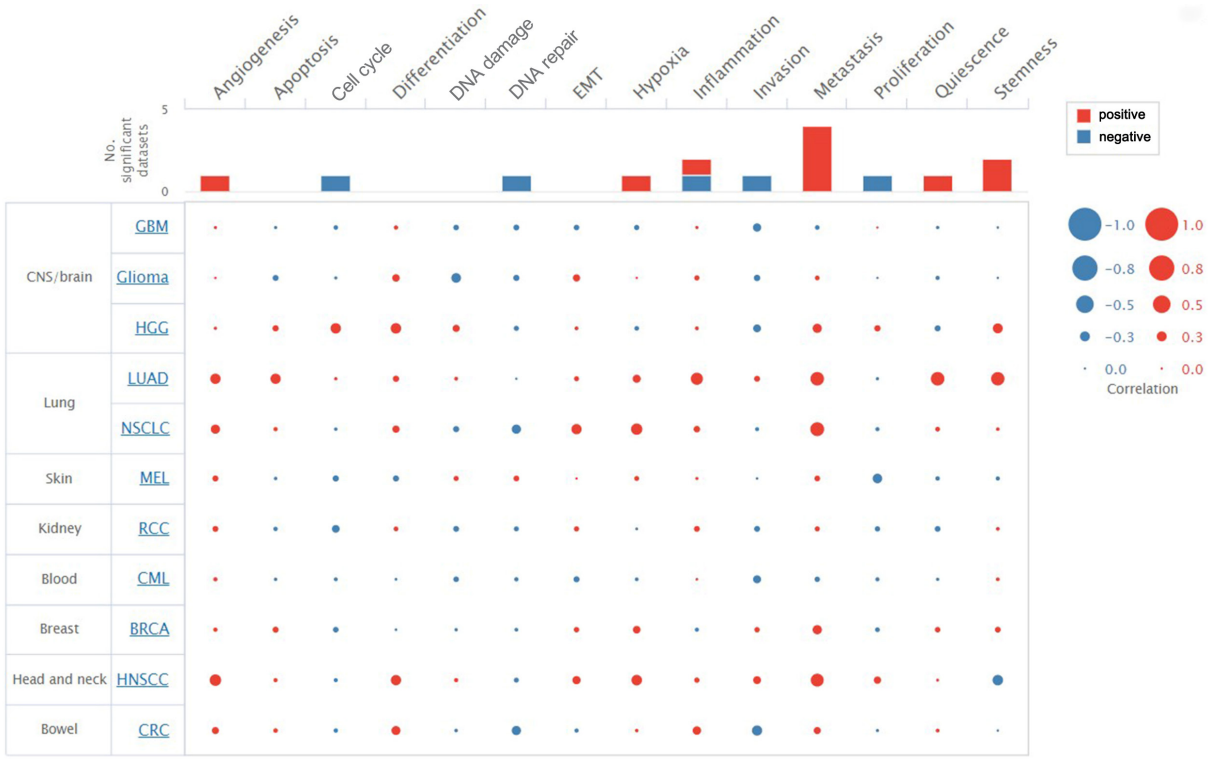

Figure S1 Functional states analysis of *ITGB4* in CancerSEA database. *ITGB4* was positively associated with most of the functional states of lung adenocarcinoma cells, especially with inflammation and metastasis in CancerSEA database. EMT, Epithelial-Mesenchymal Transition; No., Number; CNS, central nervous system; GBM, glioblastoma; HGG, high-grade glioma; LUAD, lung adenocarcinoma; NSCLC, non-small cell lung cancer; MEL, melanoma; RCC, renal cell carcinoma; CML, chronic myelogenous leukemia; BRCA, breast cancer; HNSCC, head and neck squamous cell carcinoma; CRC, colorectal cancer.

https://dx.doi.org/10.21037/tlcr-24-50

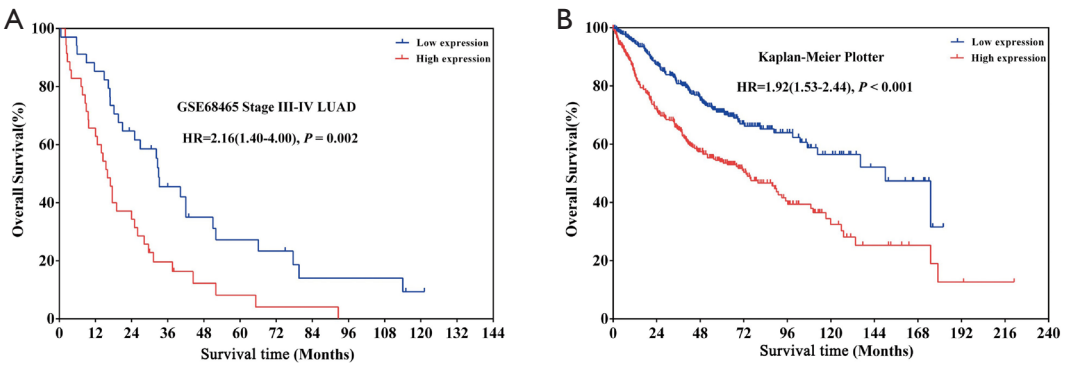

Figure S2 *ITGB4* expression is significantly associated with a worse prognosis of patients with LUAD. (A) 69 advanced LUAD patients (stage III–IV) from the GSE68465 dataset. (B) 719 LUAD patients from the Kaplan-Meier plotter (http://kmplot.com). HR, hazard ratio; LUAD, lung adenocarcinoma.

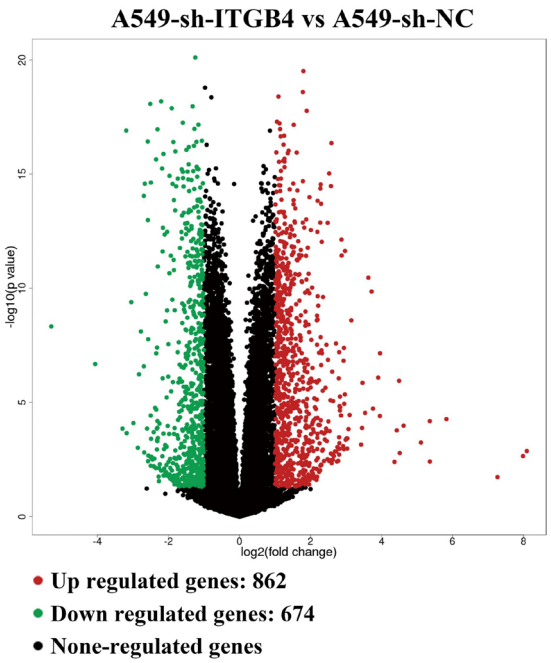

Figure S3 Volcano plot of the differentially expressed genes in RNA transcriptome sequencing data. RNA transcriptome sequencing analysis was performed to analyze the gene expression profile in A549 cells with *ITGB4* silencing. A volcano plot showed the differentially expressed genes. sh-ITGB4, short hairpin RNAs against ITGB4; sh-NC, short hairpin RNAs negative control.

https://dx.doi.org/10.21037/tlcr-24-50

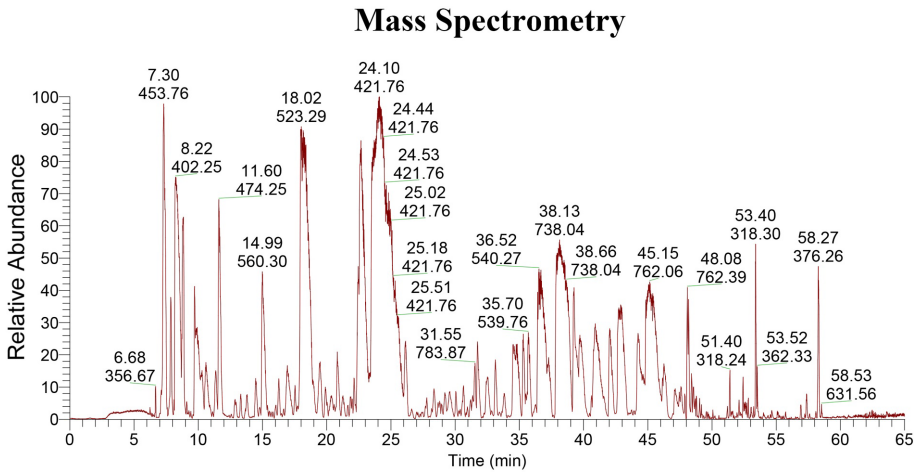

Figure S4 Mass spectrometry analysis of the proteins in the immunoprecipitation assay of *ITGB4* in A549 cells.

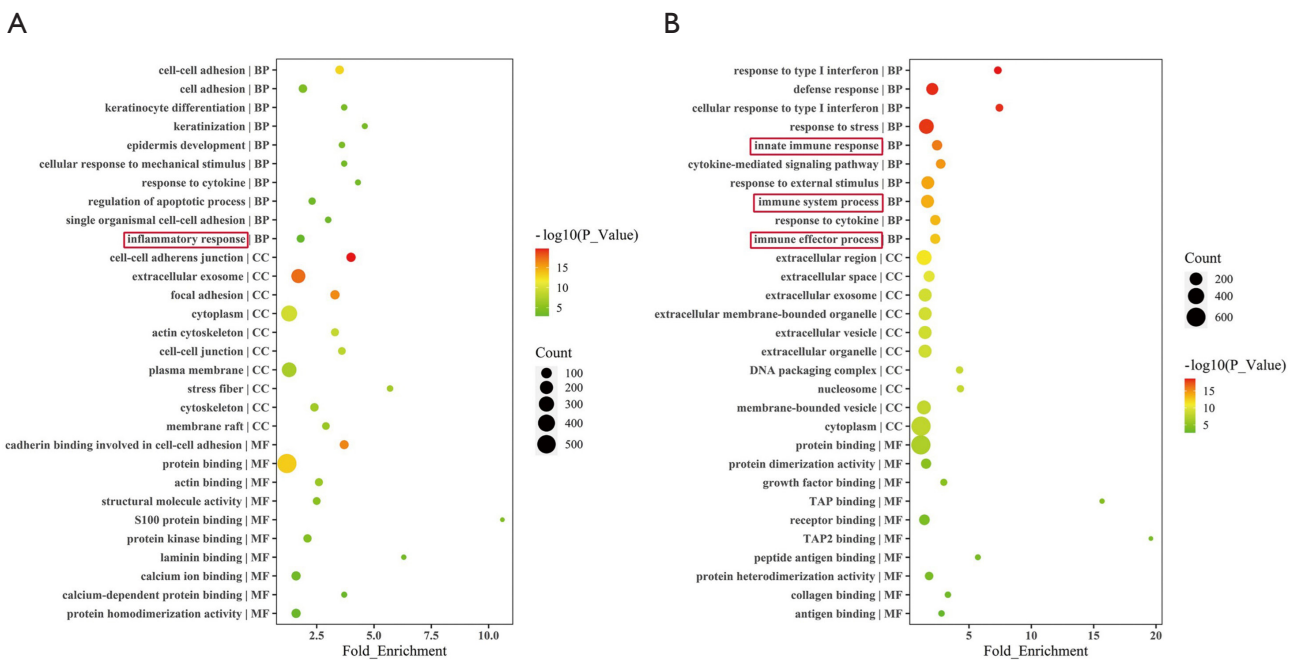

Figure S5 Gene Ontology analysis based on RNA transcriptome sequencing data and TCGA dataset. (A) Highly enriched BP term of *ITGB4* in TCGA dataset was inflammatory response. (B) Highly enriched BP terms of *ITGB4* in RNA transcriptome sequencing dataset were innate immune response, immune system process and immune effector process. TCGA, The Cancer Genome Atlas; CC, Cellular Component; MF, molecular function; BP, biological process.

https://dx.doi.org/10.21037/tlcr-24-50

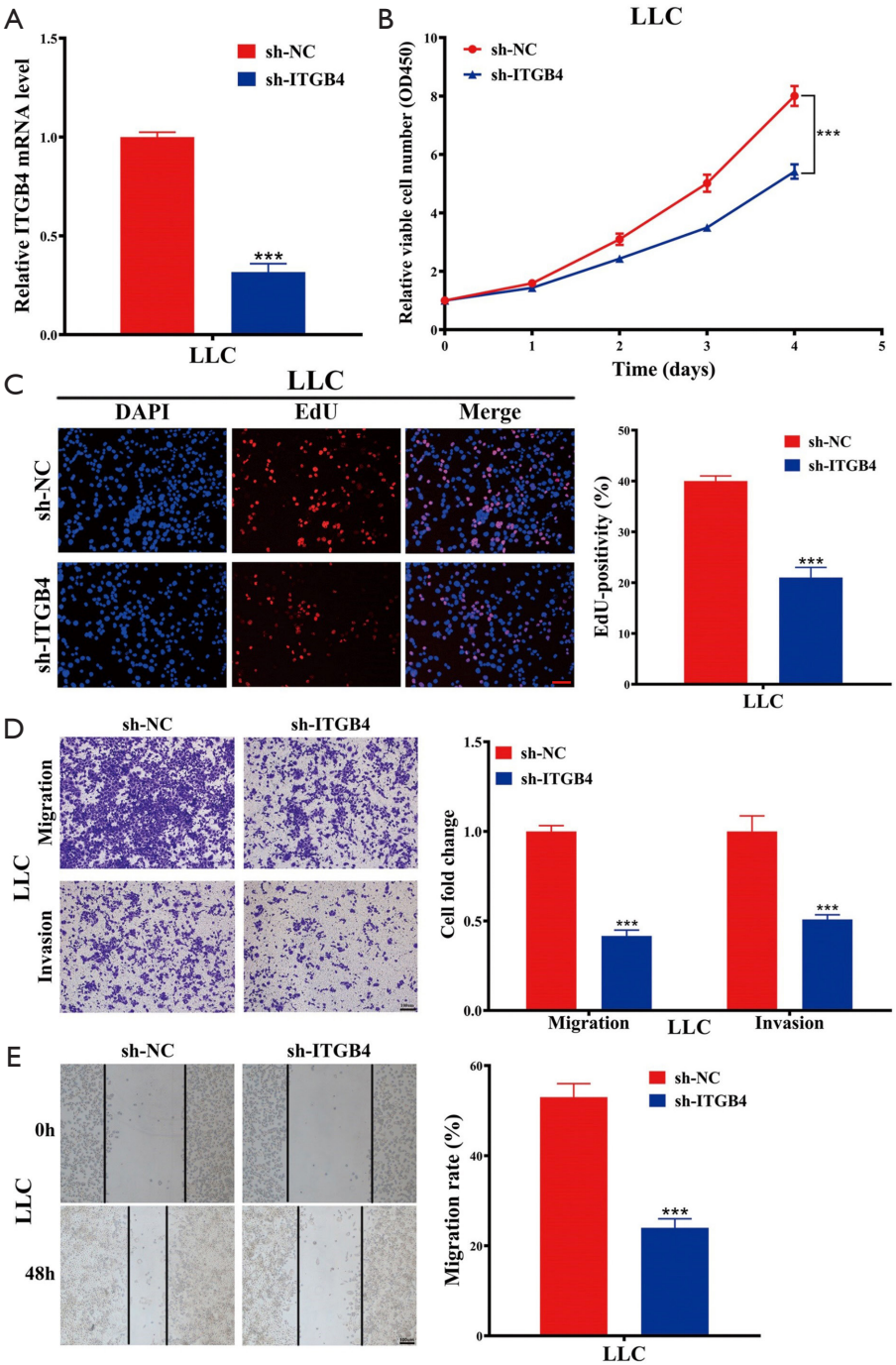

Figure S6 *ITGB4* promotes LLC cell proliferation, migration and invasion *in vitro*. (A) The effectiveness of *ITGB4* knockdown in LLC cells was confirmed by qRT-PCR analysis. (B) Cell proliferation curves were determined by CCK-8 assay after knocking down *ITGB4* in LLC cells. (C) EdU assay was conducted to evaluate cell proliferation following *ITGB4* knockdown in LLC cells. Scale bar, 50 μm. (D) Transwell assays were performed to assess the migration and invasion abilities of LLC cells upon *ITGB4* silencing. Scale bar, 100 μm. (E) Wound healing assay was carried out to evaluate the migration of LLC cells. Scale bar, 100 μm. Values are expressed as the mean ± standard deviation. *, P<0.05; **, P<0.01; ***, P<0.001. sh-ITGB4, short hairpin RNAs against ITGB4; sh-NC, short hairpin RNAs negative control; OD450, optical density at 450 nanometer; DAPI, 4',6-diamidino-2-phenylindole; EdU, 5-ethynyl-2-deoxyuridine; qRT-PCR, quantitative reverse transcription polymerase chain reaction; LLC, Lewis lung carcinoma.

https://dx.doi.org/10.21037/tlcr-24-50

Table S1 Characteristics of twenty paired lung adenocarcinoma samples used in this study

Sample ID	Gender	Age (years)	Tumor size (cm)	Subtypes	Differentiation	EGFR	Ki-67 (%)
JSPH01	Female	66	2.2	Acinar	I–II	E21 p. L858R	5
JSPH02	Male	72	5.0	Acinar	II	NA	10
JSPH03	Female	70	1.3	Acinar	I–II	E21 p. L858R	NA
JSPH04	Male	64	2.5	Micropapillary	II–III	Wild type	50
JSPH05	Male	67	2.5	Micropapillary	II–III	NA	30
JSPH06	Male	66	3.5	Solid	III	NA	60
JSPH07	Male	52	2.0	Micropapillary	II–III	NA	NA
JSPH08	Female	52	1.5	Acinar	I–II	NA	NA
JSPH09	Male	75	2.7	Papillary	II–III	Wild type	15
JSPH10	Male	73	1.6	Acinar	I–II	E21 p. L858R	5
JSPH11	Male	57	2.0	Acinar	I–II	E19	10
JSPH12	Male	50	1.5	Micropapillary	II–III	NA	NA
JSPH13	Female	55	2.0	Acinar	II	E19	NA
JSPH14	Female	56	3.0	Micropapillary	II–III	E20	25
JSPH15	Male	64	2.6	Acinar	II–III	E21 p. L858R	30
JSPH16	Male	59	2.0	Acinar	II	NA	5
JSPH17	Female	66	1.3	Solid	II–III	Wild type	20
JSPH18	Female	66	2.0	Acinar	I–II	E21 p. L858R	8
JSPH19	Female	56	1.5	Papillary	II	E21 p. L858R	NA
JSPH20	Female	58	1.3	Papillary	II	E21 p. L858R	NA

NA, not available; EGFR, estimated glomerular filtration rate.

Table S2 Sequences of siRNAs and shRNAs

Name	siRNA sequence (5' to 3')
sh-NC	TTCTCCGAACGTGTCACGT
sh-ITGB4#1 (human)	GCCTACTGCACAGACGAGATGTTCA
sh-ITGB4#2 (human)	CCTATAGCTACTACGAGAAGCTTCA
sh-ITGB4 (mouse)	CCGGCATCATGAACCGCAATGATGA
si-TFAP2A	Sense: GGGUAUUAACAUCCCAGAU
	Antisense: AUCUGGGAUGUUAAUACCCGG

siRNAs, small interfering RNAs; shRNAs, short hairpin RNAs; NC, negative control.

https://dx.doi.org/10.21037/tlcr-24-50

Table S3 Primers for quantitative reverse transcription polymerase chain reaction

Name	Primer sequence (5' to 3')
ITGB4	
Forward	CTCCACCGAGTCAGCCTTC
Reverse	CGGGTAGTCCTGTGTCCTGTA
TFAP2A	
Forward	GCTGGGCACTGTAGGTCAATC
Reverse	TGGGAGTAAGGATCTTGCGACT
β-actin	
Forward	CATGTACGTTGCTATCCAGGC
Reverse	CTCCTTAATGTCACGCACGAT

Table S4 Antibodies used in the study

Name	Company	Catalog number
ITGB4	Abcam	ab182120
p65	Abcam	ab32536
p-p65	Abcam	ab183559
IκBα	Abcam	ab32518
p-IκBα	Abcam	ab133462
IKKα/β	Abcam	ab178870
p-IKKα/β	Abcam	ab194528
TFAP2A	Abcam	ab52222
Anti-rabbit IgG, HRP-linked antibody	Abcam	ab6721
GAPDH	Abcam	ab181602
Recombinant human laminin-5 protein	Abcam	ab190413
Lamin B1	Abcam	ab133741
Anti-human CD4 antibody (IHC)	Abcam	ab133616
Anti-human CD8 antibody (IHC)	Abcam	ab245118
Anti-mouse CD4 antibody (IHC)	Abcam	ab183685
Anti-mouse CD8 antibody (IHC)	Abcam	ab217344
Ki-67	Abcam	ab279653

IgG, immunoglobulin G; IHC, immunohistochemistry.

https://dx.doi.org/10.21037/tlcr-24-50

Table S5 The top 20 proteins identified through mass spectrometry in the immunoprecipitation assay of ITGB4 in A549 cells

No.	Gene names	Unique peptides	Abundances (IP: ITGB4)	Abundances (IP: IgG)
1	*LIMA1*	15	658002991	0
2	*AIFM1*	16	456653323	0
3	*TPM4*	19	423985832	0
4	*ITGB4*	17	385194144	0
5	*DBN1*	13	285183992	0
6	*HIST1H1E*	21	227387554	0
7	*CAPZA2*	12	196453716	0
8	*CSNK1A1*	17	182016528	0
9	*UBAP2L*	11	179244107	0
10	*RPS2*	18	174538733	0
11	*KRT31*	14	153244804	0
12	*ZNF185*	12	133074577	0
13	*TNKS1BP1*	16	115573483	0
14	*NFKBIA*	13	109079161	0
15	*HNRPC*	10	90935096	0
16	*RPL18*	9	76517107	0
17	*PABPC4*	10	68809882	0
18	*DDX5*	11	55688484	0
19	*ERC1*	14	47490237	0
20	*MYO1D*	12	29366955	0

https://dx.doi.org/10.21037/tlcr-24-50